Software-Defined Radar for Monitoring and Sensing applications

Contents

Introduction

Mechanical vibrations can result from different phenomena. In many cases, they are desired effects with predictable consequences, but in some cases unwanted oscillations can occur, which interfere with other phenomena, thus causing alterations and unnecessary energy consumption. For these reasons, techniques for vibrations detection are demanded in various areas, such as industrial and civil sectors, but also in remote sensing, safety and security, as well as biomedical engineering applications. Different methods exist for the analysis of kind of phenomena, each one with specific monitoring kind. In the industrial field, the accurate vibration control of rotating machinery plays an important role in the prevention of failures of production plants. In this context, the most commonly used technologies adopt microelectromechanical systems (MEMS) or piezoelectric sensors, which are placed in direct contact with the activity source to be monitored. The mentioned approaches allow to achieve good results [1-3], but being directly subject to mechanical stresses, the sensors are exposed to wear and thus to a progressive alteration during their operation time. Optical methods, implemented with optical fibers placed at small distance from the monitored items, allow to obtain higher reliability [4-7], but similarly to the piezoelectric sensors, they generally offer operating bandwidths in the order of a few KHz [8-9], and require the use of sophisticated signal analyzers to obtain good resolutions in results.

A different solution to the use of punctual position sensors, in the context of vibrations monitoring, is given by the use of remote sensors based on coherent radars. The use of Doppler radar techniques is increasingly popular for monitoring vibrations in the civil context, such as in the remote monitoring of the dynamic characteristics of buildings [10-11]. Similar applications can be found in the biomedical field for the development of physiological sensors able to monitoring breathing and heart rate [12-13]. However, the implementation of a Doppler radar includes the use of a laboratory test equipment or custom hardware on printed/integrated circuits, and this makes the system rather bulky and expensive.

In this work, a completely new approach for Doppler radar implementation, fully based on a software-defined platform, is proposed. This alternative, flexible and low cost solution can be obtained through the use of an SDR transceiver [14-15], which leads to implement a multi-function radar, known as *Software Defined Radar*

(SDRadar) [16-17], composed by RF hardware modules fully reconfigurable via software. An SDRadar system allows to realize most of the basic operations (e.g. modulation, demodulation, filtering and mixing) by the simple use of programmable software modules, instead of specific hardware components [15], thus leading to a faster and cheaper development and manufacture, as compared to conventional custom radars [18]. The choose of a software instead of hardware platform is just performed in this work to overcome the limits imposed by electronic circuitries. As a matter of fact, while architectonic structures limit the performances in terms of detectable frequency, due to the specific (fixed) adopted hardware, our solution is strongly flexible. In particular, SDRadar is fully able to satisfy the frequency detection requirements, even in the presence of very low values (e.g. typical of heart oscillations), by simply changing via software the bandwidth, and thus the frequency detection range and the resolution. Even if many PCB and chip level realizations of custom radar sensors can be actually found at low price, the main benefit deriving from our SDRadar solution is the demonstration of using a programmable none-custom-designed RF equipment for radar motion detection study. This will enable researchers without radio frequency/ microwave circuit background to study the signal processing, system consideration, and potential applications for microwave motion sensors. The high flexibility of the proposed software architecture, essentially related to the possibility of carrying out fast detections without the need to use wearable sensors or instruments in direct contact with the item to be monitored, makes this type of systems suitable to the detection of vibrations originating from different phenomena, as those generated by industrial plants. Moreover, the proposed contactless approach can be successfully adopted for the monitoring of vital parameters, with application in security systems based on the body motion detection, or in those emergency situations for the detection of people buried under critical conditions.

State of the art

1. Contactless Technologies for Cardiorespiratory Activities Monitoring

The contactless detection of the human cardiopulmonary activity is one of the most promising solutions for sleep monitoring, post-operative surgery patients observation, domiciliary healthcare as well as applications in the safety and security field for the search and the rescue of people in emergency situations. Without contact and without some monitored subjects preparation, the health control of people suffering from chronic illnesses is significantly simplified also for the patients outside of hospital facilities. In this context, the Doppler radar used for the vital signs remote sensing has gained considerable popularity from the scientific community. The possibility to detect the vital signs, in a non-invasive and continuous way Doppler radar, has been demonstrated through a series of applications [19]. Typically, the human cardiopulmonary activity monitoring is realized through the contact sensors employment, such as the electrodes used in the electrocardiogram (ECG). In many situations, the use of these sensors is not welcome or it is not possible, as for children born premature or in those patients having serious skin impaired as the burn patients. On the other hand, contact sensors with a continuous use may suffer from a degradation, thus producing annoying cutaneous irritations, and so making ineffective and impracticable a long period monitoring.

There are manifold contexts in which a continuous and long period monitoring of vital signs could be necessary: when addressed to elderly people, or those people suffering from chronic pathologies or with sleep disorder, remote sensing of the vital signs can offer many benefits. A speedy identification of anomalies in the physiological parameters of patients may encourage an effective intervention from specialist medical staff, able to prevent heart failure with fatal consequences. The possibility to monitor, in a continuous way, the cardiopulmonary activity of these patients through contactless sensors, can have therefore an important impact in the healthcare field in terms of mortality reduction of mortality and cost reduction [20].

1.1. Traditional Methods for Cardiorespiratory Activities Monitoring

When the direct access to the patient is possible, the first option is the human supervision of cardiopulmonary function. While the ECG is certainly the 'gold' standard for the cardiac activity monitoring, an equivalent standard does not exist for the respiratory monitoring. Although the respiratory frequency is a highly premonitory parameter of patient physiological instability, its measure is often neglected for the lack of simple application monitoring methods. Typically, in fact, the respiratory frequency is manually monitored by a sanitary operator, through the visual and direct verification of the thoracic excursions.

The techniques currently used for the respiratory activity verification can be grouped into three categories: oxygen saturation measurement, airflow measurement, and respiratory movements measurement [21]. The oxygen saturation is measured through the pulse oximeter, which through a probe emitting light at different wavelength, it is able to establish how much hemoglobin is oxygen saturated. Instead, the direct airflow measurement is effected through a spirometer set in a mouthpiece or in a mask. The spirometer estimate the air volumes inspired and expired in time, but it is a tool a little used because its employment imposes an elevated effort to the patient. Airflow indirect measurements can be carried out through temperature sensors placed in proximity to the nose and the mouth. The reconstruction can be rather precise but its implementation is really annoying for the patients. The respiratory movements measurement, instead, can be carried out with various methods, by monitoring, through strain gauge or other sensors typologies, the bodily volume variation. All techniques have some types of advantages as well as disadvantages. The pulse oximeter may indicate the presence of respiratory problems, but it is not able to provide the respiratory frequency. The airflow measurements can be very accurate, but they interfere with the normal respiratory activity. The respiratory movements measurements, instead, force the patient to the immobility or to the use of wearable sensors or electrodes that degrade itself with the use.

Regarding the cardiac activity, the standard verification method, as stated above, is the ECG. This method estimates the heart muscular activity through its electric activity monitoring. The electric waves causing the heart contraction, in fact, are intercepted by electrodes placed in different chest parts and from these the heart rhythm and possible critical issues in the different heart parts can be derived. Apart from ECG, other less invasive and simpler methods exist to measure the cardiac activity. Piezoresistor or optical or pressure sensors can be adopted to monitoring the pulsations or the blood pressure, thus estimating the heart activity. All methods use, however, contact or wearable sensors.

1.2. Contactless Methods Advantages for Cardiorespiratory Activities Monitoring

The possibility to identify vital signs such as heart pulsation and respiration can be extremely useful in different circumstances in which no direct access to the subject under investigation is possible. Skin irritations, limitations in the respiration activity and contact with electrodes are conditions that in some typologies of patients, such as in the burn subjects, can be particularly critical. Beyond the health care scope, a lot of possible remote sensing applications of the vital signs are imaginable in the safety and security, for applications 'Through the wall', in search and rescue operations.

1.2.1. Patient with Serious Skin Impairment

For patients with very sensitive or extremely compromised skin, the development of reliable non-invasive techniques for the vital signs monitoring can have meaningful benefits. These situations are manifold. In the pediatric intensive care unit, the newborns often suffer from scratches and cutaneous lesion [22], due to adhesive bandages that fix the ECG electrodes. Similar difficulty situations occur in the case of fire victims. The sanitary operators often have difficulty to monitoring the heart activity of this type of patients, because they don't succeed in finding enough skin (which is not burnt), to apply the electrodes [23]. For these patients, the continuous heart activity monitoring becomes very difficult and often the esophageal echocardiogram is forced to have an idea of the cardiac system state. For the described patients typologies, it is evident that the possibility to a contactless monitoring of heart and respiratory frequency, would lead to significant advantages.

1.2.2. Sleep Monitoring

Cardiopulmonary activity is the principal parameter used in the sleep disorders study. It is widely recognized that the sleep quality and quantity have a meaningful impact on the learning, on the memory, on the cardiovascular system health, on the metabolism, and on the immune system. The apnea in the sleep (OSAS. 'Obstuctive Sleep Apnea Syndrome') is the most diffused sleep disorder and the sufferers are mostly overweight men older than forty, but the problem may affect at all ages, including the pediatric age. For apnea means the lack of airflow for great of ten seconds. The OSAS has a lot of negative consequences, among them the daytime sleepiness, the increased risk of having accidents with motor vehicle or with working equipments, the hypertension, cognitive difficulties, psychiatric nature problems.

Currently, the sleep monitoring is achieved by polysomnography, that consists in the simultaneous measurement, during the sleep, of different physiological and respiratory parameters. This practice require specific laboratory instrumentation, expensive and bulky [24], and this discourages the sleep clinics diffusion pushing downward the number of patients suffering from OSAS that receives correct treatments. The possibility to make contactless monitoring could resolve the difficulties identified and may favor the diffusion of specialist laboratories for the sleep disorder treatment, having a positive effect on the road and job accidents reduction to them referable.

The sleep apnea problems, together with other physiological parameters anomalies such as the bradycardia, are part besides, of the symptoms heralding sudden infant death syndrome (SIDS) [25]. Also for this events type, the babies sleep monitoring through contactless techniques could be extremely useful to favor a rapid intervention of healthcare professionals against harmful effects.

1.2.3. Elderly Monitoring

The elderly population, beginning from the second half of the last century, is constantly growing. It is well known that with age, older people facing the mobility reduction and the presence of equilibrium problems. These factors expose the elderly population to an elevated risk of domestic accidents caused by falls. Through contactless monitoring of the cardiorespiratory activity, would be possible to effect, in the home, continuous and long-term monitoring targeting elderly people, capable to identify conditions that requiring the healthcare professionals intervention.

1.3. Doppler Radar Employment for Human Cardiopulmonary activity Detection

The Doppler radar development for the human cardiopulmonary activity detection can conduct to the platform implementation able to effect the physiological parameters monitoring in continuous and contactless way. The Doppler radars lend themselves to detecting heart and respiratory activity also through clothes, walls or rubble. The heart and respiratory activity detection can occur simultaneously and independently.

The Doppler Continuous Wave (CW) radars ability to detect the cardiopulmonary activity has been known about 1970s [26]. In the 1980s this possibility has also been valued for Frequency-Modulated-CW (FMCW) radars and

Ultra-Wideband systems (UWB) [27-28]. The microwaves ability to effect non-invasive monitoring in the medical-diagnostic field had, in the last decades, an increasing recognition, culminated with a recent approval from the 'Food-and-Drug-Administration' (FDA). The microwaves technologies and microprocessors diffused use, within the domestic communications, drove downward this type of components costs, by making it possible the radar development for cardiopulmonary activity monitoring to more advantageous economic conditions in comparison to those offers from the traditional instrumentation.

The heart and respiratory activity monitoring, through microwaves radar, has been shown from the second half of the 1970s. In these first research jobs, the two phenomena were separately measured and this required, to the subject under observation, to hold the breath during the heart activity measurements [29]. The system used, composed by an oscillator in X band and from two horn antennas centered at the chest superior part of the subjects subject to monitoring, was able to detect the not anesthetized rabbit respiratory frequency placed to a distance of 30 cms [26]. The same system has been employed as apnea detector and it has been tested in a scenery composed by a rabbit and two anesthetized and intubated cats. This system has been able, therefore, to detect artificially induced apnea and hyperventilation conditions on the animals under observation [30].

In the 1980s and 1990s, the development of more evolved transceivers equipped with microprocessors and integrated analogical hardware, has allowed separating the weakest cardiac signal detection from the respiratory movement detection, allowing the simultaneous monitoring of the two activities, without forcing the subjects under observation to hold the breath [31]. Systems based on these transceivers use have been employed for the athletes cardiac and respiratory frequency detection [32], for buried people detection [33] or for people behind wall detection [34]. The receivers in quadrature use has allowed, besides, to resolve the 'Null Point' problem [35].

The research efforts, in the last decade, are finally moved toward the strong, light, few bulky and characterized by a low energy consumption systems development, able to carry out accurate detections to long distance, to implement portable and economic applications. The more successful use of this type of technology concerns the healthcare applications.

The experimented employments have been manifold. The use of Doppler radar has been tested for babies monitoring with the purpose to prevent SIDS events [36]. The application incorporated Doppler radar into the classical baby monitor; if this didn't detect respiratory movements in the baby for an interval of 20 sec, an alarm alert the parents. Similar solutions have been developed for a long time monitoring of the sleep apnea [37]. Different studies in sanitary area have shown the ability,

through this technology, to effect the respiratory activity monitoring in complementary or substitutive way to the conventional technologies [38].

The interest in this type of applications has pushed the scientific community to develop different architectures, optimized for different operational contexts. Various techniques are been experimented for isolating multiple target [39] and different hardware implementations hardware, with laboratory equipment [40] or with specific integrated circuits [41], have shown that this technology can be used by specialized research staff, but also from generic consumers without specific competencies in the microwaves or in RF field.

2. Radar Principle of Operation and Opportunity Provided by Doppler Effect

Radar is the acronym of 'Radio Detection And Ranging.' A radar system transmits an electromagnetic signal and observes the echo reflected by one or more objects, to get information on the presence, the position and the motion of the target intercepted. The principal functions offered by the first radar prototypes of the 1920s were essentially related to the possibility to detect some targets and to estimate the distance to which these were displaced. The scientific and technological progress has allowed, in time, to equip these systems with detection ability increasingly accurate, able to monitor more targets in simultaneously and able to track them through estimation on their speed, direction, and altitude.

2.1. Radar Background History

The radar systems radar has originally been conceived for military applications for hostile armed vehicles overseeing and control. The current applications have been extended to the civil use and they include navigation systems for vehicles aircrafts, ships, spatial nacelles, collision avoidance systems for cars, precipitations monitoring applications, radio astronomy and geologic observation applications, together with the classical military applications for aerial defense as the missile defence systems or the guidance systems for missile. The way for the electromagnetic waves use has been made from James Clerk Maxwell, that formulated the unified theory of the classical electromagnetism around 1860 and from Heinrich Hertz that it was the first one to show the radio waves transmission and reflection around 1880. The reflected electromagnetic waves for individualizing objects has not been used until the early 1900s, when through the

Doppler effect, described by Christian Andreas Doppler in 1842 [42], Christian Huelsmeyer and Nikola Tesla individualized distant moving boats. In the 1920s, Albert Hoyt Taylor of the 'Naval Research Laboratory' developed a radar for the naval tracing, installed on board of a boat in 1937 [43]. In 1924, Sir Edward Victor Appleton used the technology now known as 'Frequency-Modulated Continuous Wave', FMCW, to show the ionosphere existence and to measure its distance [44]. A big contribution in the radar systems evolution has been surely brought by Sir Robert Alexander Watson Watt, which developed, on behalf of the 'British Meteorological Office', the first radar for meteorological purposes. Particularly Sir Watt realized a radar able to detect the presence of distant stormy phenomena. All the Sir Wat studies carried him to have a decisive role for the Second World war results. On behalf of the 'British War Office' Sir Watt developed, in fact, a radar system able to individualize hostile military airplanes before these were visible, obtained the patent for the first pulsated radar system. Beginning from 1939, and throughout the Second World war, Great Britain prepared a series of radar stations along its coasts to detect the aerial or maritime vehicles possible arrival. During the war technology had a significant evolution and the first systems equipped with display were also predisposed to a rapid and simplified radar signals reading.

Finished the Second World war the radar technology was, therefore, used in various civil sectors coming so, to our days, present in a variegated applications range.

2.2. Radar Principle of Operation

When a radar system transmits a radio frequency (RF) energy impulse, a small portion of this is reflected by the intercepted objects and it comes back following the same path. Since the electromagnetic waves speed in free space is equal to the light speed, it is possible to derive the intercepted objects distance by the measurement of the time interval between the transmission and the receipt, by the radar, of the reflected signal. If the radar system is also able to measure the reflected electromagnetic wave frequency, it is possible to derive the object speed from the frequency shift suffered by the transmitted signal. The principal advantage of the electromagnetic waves use, particularly if they are located in the microwaves spectrum, is represented by their ability to penetrate clouds, smog, and dust, detecting also nonvisible objects [43].

As shown in Figure 1, a radar system is macroscopically composed by a transmitter, an antenna, a receiver and a unity devoted to the signals elaboration. The transmitter produces the electromagnetic wave, and through amplifiers, it gives them the necessary power. An antenna, typically an electronic scanning antenna

array, focus the energy in the target direction. The receiver picks up the reflected signal, filters it from noises and move it in baseband to forward it to the elaboration unity devoted to the information extraction.

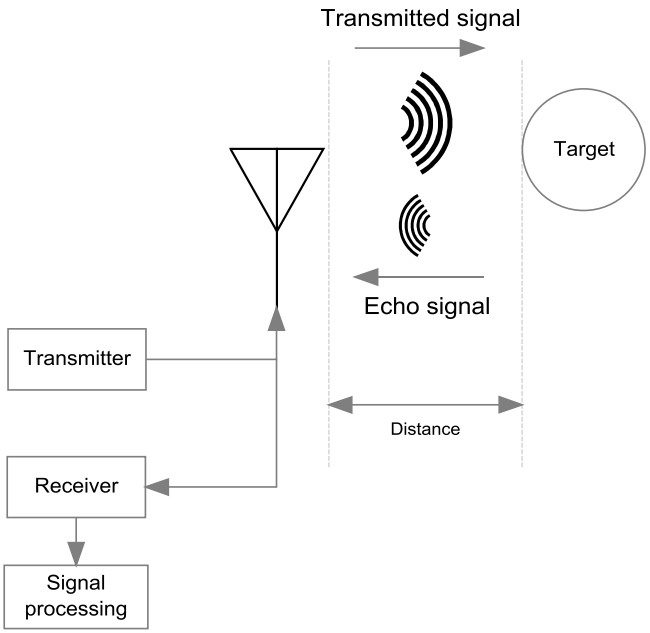

Figure 1 - Radars principle of operation

In principle, the radars can operate at any frequency but the practical implementation, in terms of antenna dimension, transmitted power, distance from the target and resolution, impose some constraints on the working frequency. The frequency range conventionally employee for RF applications is from 3 KHz to 300 GHz, but the 'IEEE Standard for Letter Designation for Radar-Frequency Bands' has identified the 3 MHz-300 GHz range as a useful band for radar applications.

2.3. Radar Doppler

The Doppler radars are typically used for individualizing objects in movement and to estimate their speed. The most common applications of Doppler radars concern the meteorological images extraction and the vehicles speed detection. Another typical context in which the Doppler radars are used is the safety and security context. In these applications the Doppler radars are used for fixtures movements or opening detection to indicate possible intrusions.

2.3.1. Doppler Effect

The Doppler effect, or Doppler shift, is the frequency variation of the received wave when the observer is in movement in comparison to the same. This

phenomenon was discovered by the German physicist Christian Doppler and concerns all the wave types, included the sound waves, light waves, and electromagnetic waves. If the sound frequency coming from a source maintains constant, and both the source and the observer stay in their position, the sound wave maintains the original frequency and the observer it receives the same number of produced wavefronts. If instead the source or the observer reach toward, the observer perceives a higher frequency sound because, in the same time frame, he collects more wavefronts. In analogous way, if the source or the observer moving away, the observer perceives a lower frequency sound because he collects fewer wavefronts.

Considering R as target distance and λ as wavelength, the number of wave collects, coming from the target and intercepted by the radar will be $2R/\lambda$. To every wavelength corresponds a 2π radians variation. The total phase delay, in roundtrip it is therefore equal to that shown in eq. (1).

$$\phi = 2\pi \times \frac{2R}{\lambda} = \frac{4\pi R}{\lambda} \tag{1}$$

The target movement in relation to the radar position will produce therefore a phase variation. Deriving with respect the time, as shown in the eq. (2), you get, therefore, the speed with which the phase changes and therefore the angular frequency

$$\omega_d = \frac{d\phi}{dt} = \frac{4\pi}{\lambda}\frac{dR}{dt} = \frac{4\pi v_r}{\lambda} = 2\pi f_d \tag{2}$$

where $v_r = dR/dt$ indicates the radial speed (m/s) or the speed with which the distance varies in time. If, as shown in Figure 2, the angle between the target vector speed and the radar line of sight of is θ, then radial speed is that shown in the eq. (3)

$$v_r = v\cos\theta \tag{3}$$

where v is the speed or the vector magnitude. From eq. ((2) may be derived the Doppler shift as shown in the eq. (4)

$$f_d = \frac{2v_r}{\lambda} = \frac{2f_t v_r}{c} \tag{4}$$

where f_t is the transmitted signal frequency by the radar and c is the light speed ($3 \times 10^8 m/s$).

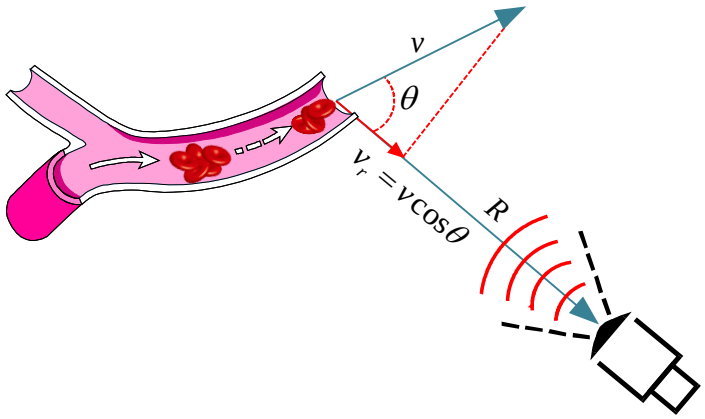

Figure 2. Target movement speed in relation to the radar

2.3.2. Radar Doppler Waveforms: CW, FMCW, Pulsed

2.3.2.1. Continuous Wave

A CW radar, is a system that in continuous way transmits and receives a very narrow band signal. The transceiver CW is characterized by a very simple topology composed by a transmitter and a receiver heterodyne or homodyne. As the transmission and the receipt are continuous, these systems do not require a control that selects the receipt and transmission channel as in the pulsated radars case [45]. A CW radar may be equipped with a single antenna accompanied by a duplexer or by a circulator to isolate the transmitted signal and the received one, or it can use separate antennas to transmit and to receive. Since the band is extremely narrow, the filters used in the different stadiums are very simple, and the Doppler shift results very evident. Theoretically, a CW radar system may recognize, in nonambiguous way, the rate of a target placed at any distances with any speeds.

The principal disadvantage of the CW radars is represented by the losses between the transmitter and the receiver. A portion of the transmitted signal, because of the losses, pairs in the receiver through the circuitry or directly through the antennas. These losses inject in the receiver a big signal characterized by the same frequency of the transmitted one, that is not related to any targets presence. The presence of others signals at the same frequency of the transmitted one may also be linked to other objects that don't result of interest or from static target. These not desider signals cause a DC component and low-frequency noise that are not upstream eliminable.

A CW radar system with single-ended receiver is not able to distinguish if the target is in approach or in leaving because it is not able to preserve the shift direction

information in the conversion phase from the bandpass to the baseband. To remedy this problem, coherent heterodyne or in quadrature homodyne receivers are used, which succeed in estimation of the target movement direction [44].

2.3.2.2. FMCW

A CW Doppler radar is able to determine the target speed by identifying CW received signal frequency shift. To the purpose to not only detect the speed but also the target range, is necessary that the used signals are syncronized in some form, in such way to be been able for measure the delay between the transmitted signal and the received one. To resolve this problem, it is possible to introduce different CW signals modulation types as the FMCW modulation, 'Stepped Frequency Continuous Wave' (SFCW) modulation, 'Coded Modulation' (CM), 'Noise Modulation' (NM), 'Synthesized Pulse Modulation' (SPM), 'Holographic Modulation' (HM) or 'Amplitude Modulation' (AM) [46].

The modulation in frequency more commonly used for the systems FMCW is that triangular, in which the frequency variations are gradual. In Figure 3 is shown a frequency modulation in an FMCW radar example. The transmitted signal is represented by the continuous line, while the dotted line shows the backscattered signal frequency received by a static target. The frequency excursion Δf is the FMCW signal band and determines the maximum obtainable accuracy on the distances detected, while the repetition frequency of the triangular modulation f_m determines the maximum unambiguous range. The reflected signal reaches the radar with a delay, by comparison to the transmission, expressed by the eq. ((5)

$$T = \frac{2R}{c} \tag{5}$$

where R is the target range. The received signal and the transmitted one are multiplied in a mixer that produces a signal out with a f_b frequency equal to the frequencies difference of the mixed signals.

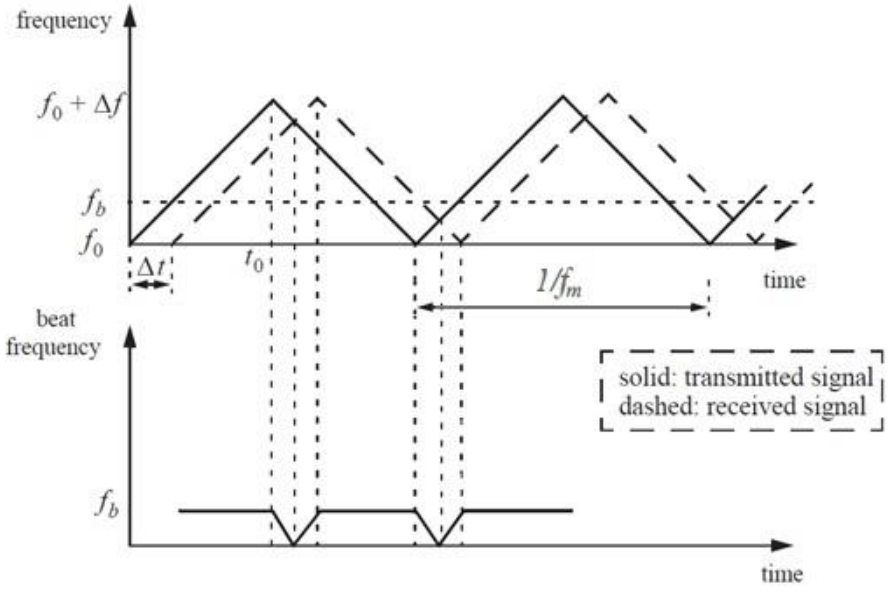

Figure 3 - Transmitted and received signal, and beat frequency individualized by a FMCW radar for a static target (courtesy of [47])

In the example shown in Figure 3, the frequency shift f_b is entirely due to the target range R effect, express as f_r. From simple geometric considerations can be determined f_b as shown in the eq. (6).

$$f_b = f_r = \frac{4Rf_m\Delta f}{c} \tag{6}$$

With the presence of moving target, f_b results determined, as well as by f_r, also from f_d that represents the due move to the Doppler effect. In this case, the frequency difference is $f_r + f_d$ during a half period of modulation and $f_r - f_d$ during the other half period, as shown in Figure 4. The target range may be obtained as the average among these two frequencies in the $1/f_m$ period.

The FMCW radar resolution, in terms of distance, is express from the eq. (7).

$$\Delta R = \frac{c}{2\Delta f} \tag{7}$$

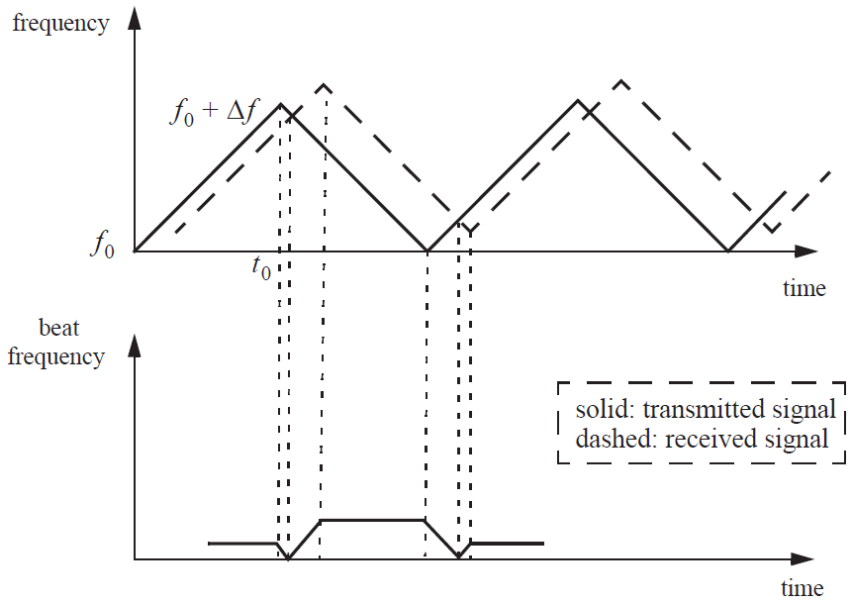

Figure 4 - Transmitted and received signal, and beat frequency individualized by a FMCW radar for a moving target (courtesy of [47])

An application example is described in [48], where a FMCW radar system has been used as altimeter on board of an aircraft.

2.3.2.3. Pulsed Doppler Radar

The pulsed radars are the radar category mostly used. A pulsed radar transmits narrow impulses, characterized by elevated power, to a repetition frequency, PRF, constant; from the analysis of the time employed by the impulse reflected by the target to return back, the intercepted target range can be reconstructed. The pulsed radars that use the Dopper effect for the moving target detection are called "Moving Target Indication" - MTI radar or pulsed Doppler radar [48]. The technique mostly used, for the range reconstruction with this radar typology, provides for measure the delay between the transmitted impulse and the reflected impulse receipt. Since the RF energy is propagated with light speed, the τ delay between the impulse transmission and receipt has shown in the eq. (8).

$$\tau = \frac{2R}{c} \tag{8}$$

The principal pulsed radars advantage in comparison to the CW or FMCW radars is the possibility to have quite separate times of transmission and receipt, allowing to avoid involvement of the weak echoes receipted caused by the losses, in the transmitter, of the strongest transmitted signals.

If the impulse duration is sufficiently long and the target speed is enough elevated, it is possible, also in the pulsed radars, to detect the frequency shift for Doppler effect through the single impulse duration variation and the impulses sequence PRF variation.

3. Software-Defined Radio

Generally, radio systems have been engineered to process a specific signal or waveform. Single-function radio system that operate in a known and fixed environment are easy to optimize for performance, size, and power consumption. Most home radio systems, at a superficial analysis, appear to be single function but many of these devices are actually quite flexible and support different waveforms. The software-defined radio's (SDR) main characteristic is, therefore, its ability to support different waveforms by using the same hardware platform in which some or all of the physical layer functions are software defined. An ideal and basic block diagram of this type of radio systems is shown in Figure 5, in which the software running on a custom or general purpose microprocessor selects one of the system function available to it, with this functionality no explicitly included by the designers.

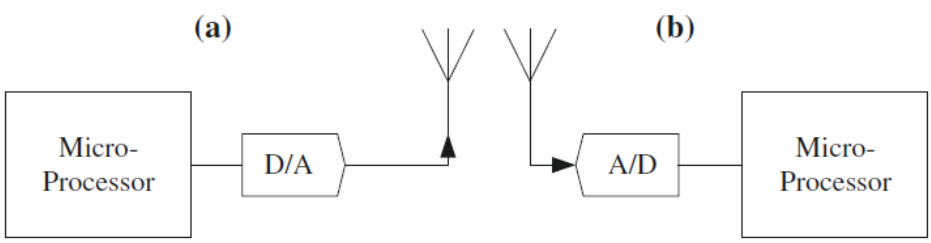

Figure 5 - Ideal software-defined radio system: (a) TX stage, (b) RX stage (courtesy of [49])

The digital samples are then converted directly into an RF signal and sent to the antenna. The transmitted signal enters the receiver at the antenna, is sampled and digitized, and finally processed in real time by a general purpose processor. Ideally, the SDR hardware should support any waveform at any carrier frequency and any bandwidth, but in reality there are some limits, such as the difficulty to tune antennas dynamically. The band of interest extension also requires wideband antenna, and if this are available, places high demands on the RF front end, the A/D converters and the real-time digital signal processing.

Some of the most significant advantages and applications are summarized below.

- *Interoperability*. An SDR can seamlessly communicate with multiple incompatible radio system or act as a bridge between them.

- *Optimized use of resources according to the operational context.* An SDR can use the appropriate waveform to maximize the systems performances for every scenario. For example, a low-power waveform can be used if the system battery is running low, or high-throughput waveform can be selected to quickly download a large file.
- *Cognitive radio.* An SDR can reuse the frequency in opportunistic way. If a specific band is momentarily available, an SDR can use the spectrum until the owner comes back. This technique dramatically increase the amount of available spectrum.
- *Reduced obsolescence.* An SDR can be upgraded in the field to support the latest communications standards, saving the new hardware and its installation cost.
- *Lower cost*. An SDR can be adapted for multiple markets and applications. Economies of scale have a cost of each device reducing effect.
- *Research and development.* An SDR can be used to implement many different waveforms for real-time performance analysis. Large trade-space studies can be conducted much faster than through simulations.

The technology is not without disadvantages and ambiguity.

- *Device cost for simple application.* This aspect is particularly important for high-volume, low margin consumer products, for example a garage or car door remote opener key fob or AM/FM radio receivers. These extremely simple devices are also high-volume and potentially very low cost. An SDR is necessarily more complex than these single-function radio and also employing SDR chip for the above applications, the increased market volume would not drive chip cost sufficiently down.
- *Power.* In an SDR system there are two sources contributing to higher power consumption: increased processor complexity and higher mixed-signal/RF bandwidth. FPGA used to implement flexible signal processing and wideband ADCs/DACs consume more power than ASIC microprocessor and narrowband ADCs/DACs generally used in single-function radio.
- *Complexity.* An SDR requires additional complexity compared to a standard radio system. It takes more engineering effort to develop software and firmware to support flexible waveform than to support fixed one and it impacts on time and cost to implement the SDR platform.

3.1. Universal Software Radio Peripheral

The Universal Software Radio Peripheral (USRP) introduction drive down the SDR device cost from tens of thousands dollars to hundreds dollars. The USRP is a commercial product developed since 2010 by Ettus Research, a little research company, that was then acquired by National Instruments (NI). USRP was released at about the same as GNURadio with drivers source code and mixed-signal circuit board in the public domain but RF circuit boards are proprietary. USRP is currently supported in MathWorks Simulink and NI LabView.

The first USRP model is equipped with an USB 2.0 interface and provides up to 30 MHz of instantaneous bandwidth for about $1000 (Figure 6).

Figure 6 - First USRP model (USRP1)

The second USRP model is equipped with a gigabit Ethernet interface allowing it to increase instantaneous bandwidth to 50 MHz at about $2000 (Figure 7).

Figure 7 - Second USRP model (USRP2)

Different daughter boards are used to support a range of frequencies from DC to 6 GHz. Each USRP supports two receive and two transmit channels and multiple USRPs can be synchronized to provide more coherent channels. The USRP consist of an FPGA, 100 MHz-class A/Ds and D/As, RF daughter boards and an interface to the host computer (Figure 8). The FPGA is used to channelize the data and interface to the host port.

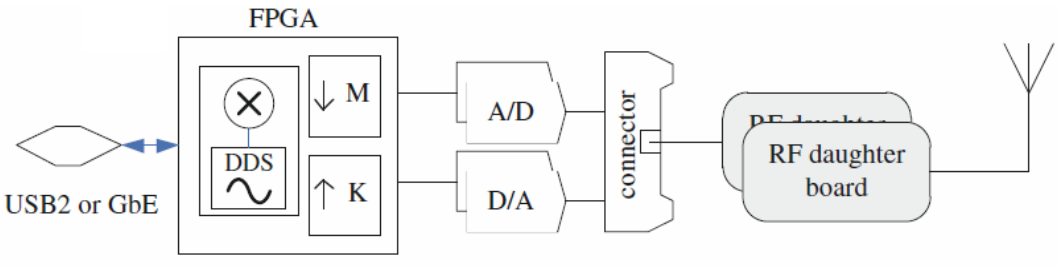

Figure 8 - USRP block diagram

The FPGA implements digital frequency shifting and rate change. The FPGA source code can be modified to implement more sophisticated processing. Some or even all of the processing for the SDR application can be implemented on the FPGA to achieve higher throughput than it possible with a PC [50].

Support Theory

1. Doppler Radar Continuous Wave: Principle of Operation

The wave reflected by a moving object, whatever its physical nature is, suffers a frequency shift, compared to the incident wave on the same, proportional to the object speed. This phenomenon, known as effect Doppler, is exploited in the radars to individualize moving target and eventually to monitoring their motion. You suppose to use a transceiver, working in the microwaves spectrum, able to transmits a monochrome signal with f_0 frequency, characterized by a $\theta(t)$ phase noise (eq. (9)).

$$Tx(t) = \cos[2\pi f_0 t + \theta(t)] \tag{9}$$

The generated signal, during propagation, intercepts an objective to a d_0 nominal distance that causes its backscattering. The backscattered signal, recovered by the receiver, results attenuated by L propagation losses factor and is correlated to the transmitted signal through the $\tau(t)$ delay (eq. (10)). This delay induces, in the received signal (eq. (11)), a frequency shift, known as f_d Doppler frequency, linearly related to the intercepted object radial speed v_r, as shown in the eq. (12).

$$\tau(t) = \frac{2d_0}{c} + \frac{2v_r}{c}t \tag{10}$$

$$\begin{aligned} Rx(t) &= L \cdot Tx\big(t-\tau(t)\big) = L \cdot \cos\big[2\pi f_0\big(t-\tau(t)\big) + \theta\big(t-\tau(t)\big)\big] = \\ &= L \cdot \cos\left[2\pi f_0 t - \frac{4\pi f_0 d_0}{c} - \frac{4\pi f_0 v_r}{c}t + \theta\big(t-\tau(t)\big)\right] = \\ &= L \cdot \cos\left[2\pi\left(f_0 - \frac{2v_r}{\lambda}\right)t - \frac{4\pi d_0}{\lambda} + \theta\big(t-\tau(t)\big)\right] = \\ &= L \cdot \cos\left[2\pi(f_0 + f_d)t - \frac{4\pi d_0}{\lambda} + \theta\big(t-\tau(t)\big)\right] \end{aligned} \tag{11}$$

$$f_d = -\frac{2v_r}{\lambda} \tag{12}$$

Through the received and the transmitted signals treatment, it is possible to extract the intercepted object speed information. In fact, when they are multiplied through a mixer and then filtered, through a pass-low filter, the baseband signal in resultant exhibits a frequency equal to f_d therefore linearly related to the target speed (Figure 9).

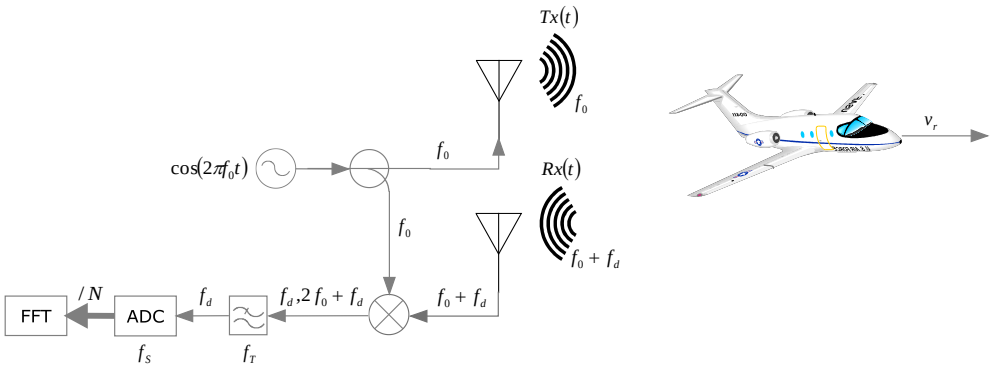

Figure 9 - Doppler Continuous Wave (CW) radar architecture

Out of filter, after the interest signal analogical-digital conversion, it is possible to extract the f_d frequency shift through a Fast Fourier Transform (FFT) algorithm. Finally, by eq. (12), it is possible to reconstruct the intercepted object radial speed.

The Doppler CW radar described is characterized by some important parameters:

- B is the receiving antenna bandwidth;
- f_T it is the low-pass filter cutoff frequency. This parameter limits the maximum detectable speed and is in relationship with receiving antenna bandwidth by eq. (13);

$$f_T \geq \frac{B}{2} \tag{13}$$

- f_S is the sampling frequency of the analogical-digital conversion circuit and it must be chosen so as to satisfy the Nyquist-Shannon sampling theorem according to the relationship expressed by the eq. (14);

$$f_S \geq 2f_T \tag{14}$$

- T_0 is the time period of every acquisition interval;
- N expresses the collected samples number in an T_0 acquisition interval. The collected samples are subsequently transferred from the analogical-digital conversion circuit to the FFT processing block. The samples number can be evaluated by the eq. (15).

$$N = T_0 f_s \tag{15}$$

There are some useful relationships useful to bind these radar parameters to its characteristics in resolution and maximum detectable frequency terms. From eq. (15) it is possible to determine the resolution (eq. (16)), while the maximum detectable frequency is determined beginning from the low-pass filter cut-off frequency and from the receiving antenna bandwidth (eq. (17)).

$$\Delta_f = \frac{f_s}{N} = \frac{f_s}{T_0 f_s} = \frac{1}{T_0} \tag{16}$$

$$f_{max} = f_T = \frac{B}{2} \tag{17}$$

By eq. (12) the speed resolution can be derived (18) and the maximum detectable speed (19).

$$\Delta_v = \frac{\lambda}{2T_0} \tag{18}$$

$$v_{max} = \frac{\lambda B}{4} \tag{19}$$

2. Doppler Radar CW for Vibrations Monitoring

The architecture presented can be used in different application contexts than those above. This type of radar, in fact, characterized by a very simple, sturdy and reliable architecture, based on a single local oscillator and narrowband signals, can be exploited for the oscillatory motions monitoring. In this case, hypothesizing in the reference scenario the presence of only one oscillating object oscillations, it is possible to individualize two parameters that characterize the target motion:

- $x(t)$, that describes the target oscillatory motion;
- d_0, that represents the distance from the radar, around which the target vibrate.

Figure 10 shows the described scenario diagram.

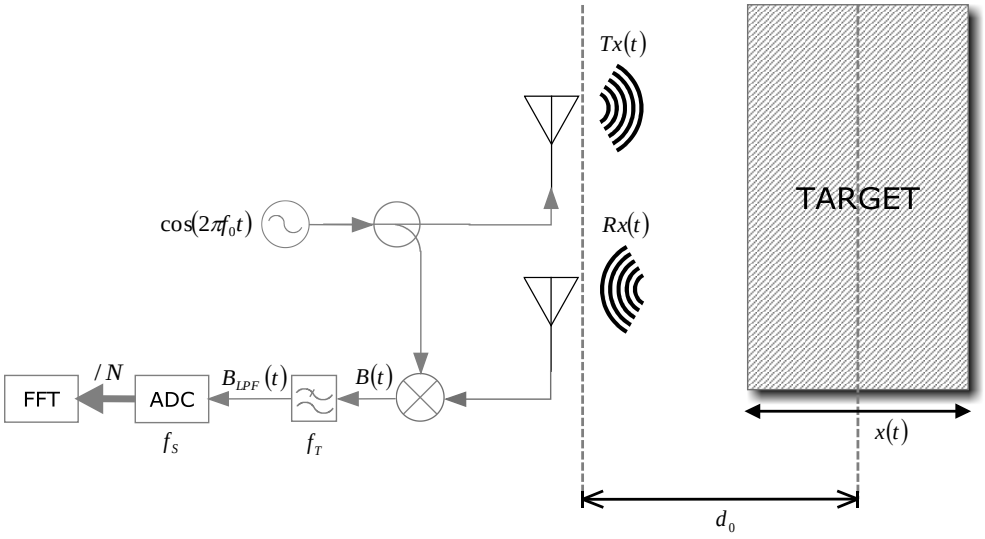

Figure 10 - Typical scenario for the vibration monitoring applications through Doppler CW radar

It is possible to define the time function that describes the distance between radar and target as shown in eq. (20)

$$\bar{x}(t) = d_0 + x(t) \tag{20}$$

Beginning eq. (20), can be obtained the time spent by electromagnetic wave, transmitted by the radar, to intercept the target and to return back after having been reflected, known as 'Round Trip' time (eq. (21)).

$$\tau(t) = \frac{2\bar{x}(t)}{c} = \frac{2d_0}{c} + \frac{2x(t)}{c} \tag{21}$$

where c represents the lightspeed in the vacuum.

The backscattered signal, received from the radar, has the same form of the transmitted signal, shown in the eq. (9), attenuated by a L factor that, as described above, model the propagation losses, and delayed by $\tau(t)$ (eq. (21)). The eq. (22) provides the exposed analytical formulation.

$$\begin{aligned} Rx(t) &= L \cdot Tx\big(t - \tau(t)\big) = L\cos\big[2\pi f_0\big(t - \tau(t)\big) + \theta\big(t - \tau(t)\big)\big] = \\ &= L\cos\left[2\pi f_0 t - \frac{4\pi f_0 d_0}{c} - \frac{4\pi f_0 x(t)}{c} + \theta\left(t - \frac{2d_0}{c}\right)\right] \end{aligned} \tag{22}$$

Defining α, β and γ as shown in the eqs. (23)-(25)

$$\alpha = 2\pi f_0 t \tag{23}$$

$$\beta = \frac{4\pi f_0 d_0}{c} \tag{24}$$

$$\gamma = \frac{4\pi f_0 x(t)}{c} \tag{25}$$

it is possible to express the eqs. (9) and (22) in compact form as shown in eqs. (26) and (27).

$$Tx(t) = \cos[\alpha + \theta(t)] \tag{26}$$

$$Rx(t) = L\cos\left[\alpha - \beta - \gamma + \theta\left(t - \frac{2d_0}{c}\right)\right] \tag{27}$$

The obtained signal after the transmitted and the received signal mixing is shown in eq. (28).

$$\begin{aligned} B(t) &= Tx(t) \cdot Rx(t) = \\ &= L\left\{\cos\left[2\alpha - \beta - \gamma + \theta(t) + \theta\left(t - \frac{2d_0}{c}\right)\right]\right. \\ &\left. + \cos\left[\beta + \gamma + \theta(t) - \theta\left(t - \frac{2d_0}{c}\right)\right]\right\} \end{aligned} \tag{28}$$

Out of low-pass filter, downstream of the mixer, the signal is as shown in the eq. (29).

$$B_{LPF}(t) = L\cos\left[\beta + \gamma + \theta(t) - \theta\left(t - \frac{2d_0}{c}\right)\right] \tag{29}$$

Replacing in the eq. (29) the eq. (24) and (25) and declaring the λ wavelength and the $\Delta\theta(t)$ residual phase noise as in eqs. (30) and (31)

$$\Delta\theta(t) = \theta(t) - \theta\left(t - \frac{2d_0}{c}\right) \tag{30}$$

$$\lambda = \frac{c}{f_0} \tag{31}$$

it is possible to express the signal in out of low-pass filter as shown in eq. (32).

$$B_{LPF}(t) = L\cos\left[\frac{4\pi d_0}{\lambda} + \frac{4\pi x(t)}{\lambda} + \Delta\theta(t)\right] \tag{32}$$

The signal expressed by eq. (32) includes, evidently, information on the intercepted object oscillatory motion, determined by the presence of the $x(t)$ function in the cosine argument. It is necessary, therefore, to elaborate this signal

to reconstruct and to study the intercepted object motion. As already been extensively discussed in literature, [51-52], different factors, related to the scenario conformation and composition, influence these informations extraction, among them the phase delay introduced from the intercepted object surface and from the wirings between the components, and the distance between target and antennas.

By defining θ_0 in eq. (33)

$$\theta_0 = \frac{4\pi d_0}{\lambda} \tag{33}$$

and neglecting the $\Delta\theta(t)$ phase residual noise, may be identified two different conditions, known as 'Optimum Detection Point' and 'Null Detection Point', the first one allows to have an optimal sensibility for the target motion extraction, the second one doesn't allow to get reliable reconstructions. The occurrence of these conditions is related to the d_0 distance between target and radars antennas. Particularly 'Optimum Detection Point' is when the d_0 distance is such to be verified the condition expressed by eq. (34).

$$\theta_0 = \frac{4\pi d_0}{\lambda} = \frac{\pi}{2} + k\pi \quad \forall k \in \mathbb{N} \tag{34}$$

For which adopted earlier, assuming that the d_0 distance respects the condition expressed by eq. (34), it is possible to re-phrase eq. (32) as shown in eq. (35).

$$B_{LPF}(t) = L\cos\left[\theta_0 + \frac{4\pi x(t)}{\lambda}\right] = L\sin\left[\frac{4\pi x(t)}{\lambda}\right] \tag{35}$$

In this case, assuming that the motion oscillatory amplitude is very smaller than the λ wavelength (eq. (31)), it is possible to effect a trigonometric approximation of the eq. (35), known as 'Small Angle Approximation', getting a signal in direct proportionality relationship with the intercepted target oscillatory motion, as shown in eq. (36).

$$B_{LPF}(t) = L\frac{4\pi x(t)}{\lambda} \tag{36}$$

In the 'Optimum Detection Point' condition, it is therefore possible to correctly reconstruct the target motion through the expression shown in the eq. (37), obtained from eq. (36), using the architecture shown in Figure 10.

$$x(t) = \frac{1}{L} \cdot \frac{\lambda}{4\pi} \cdot B_{LPF}(t) \tag{37}$$

Nevertheless, because of the second condition mentioned above, in some circumstances this architecture is not able to effect reliable reconstruction of the intercepted object oscillatory motion. Particularly, a 'Null Detection Point' is when d_0 distance is such that condition expressed by the eq. (38) is verified.

$$\theta_0 = \frac{4\pi d_0}{\lambda} = \pi + k\pi \qquad \forall k \in \mathbb{N} \tag{38}$$

In this case, assuming that the d_0 distance respects the condition expressed by the eq. (38), it is not possible to re-phrase the eq. (32) as shown in eq. (35), therefore achieving, the expression shown by eq. (39).

$$B_{LPF}(t) = L\cos\left[\theta_0 + \frac{4\pi x(t)}{\lambda}\right] = L\cos\left[\frac{4\pi x(t)}{\lambda}\right] \tag{39}$$

Also in this case it is possible to apply 'Small Angle Approximation.' The obtained signal, shown in the eq. (40), it doesn't result linearly proportional to the intercepted object motion.

$$B_{LPF}(t) = L\left\{1 - \frac{1}{2}\left[\frac{4\pi x(t)}{\lambda}\right]^2\right\} \tag{40}$$

Insofar, in the 'Null Detection Point' condition, the described architecture is not able to effect a correct target motion reconstruction through the eq. (37), exposing therefore a notable sensibility diminution.

From eqs. (34) and (38) it is possible to derive the 'Optimum Detection Point' (eq. (41)) and the 'Null Detection Point' (eq. (42)) dislocation express in relation with the wavelength.

$$d_{0_{OPTI}} = \lambda\left(\frac{1}{8} + k\frac{1}{4}\right) \quad \forall k \in \mathbb{N} \tag{41}$$

$$d_{0_{NULL}} = \lambda\left(\frac{1}{4} + k\frac{1}{4}\right) \quad \forall k \in \mathbb{N} \tag{42}$$

The points distribution, in relation to the wavelength, is represented in Figure 11.

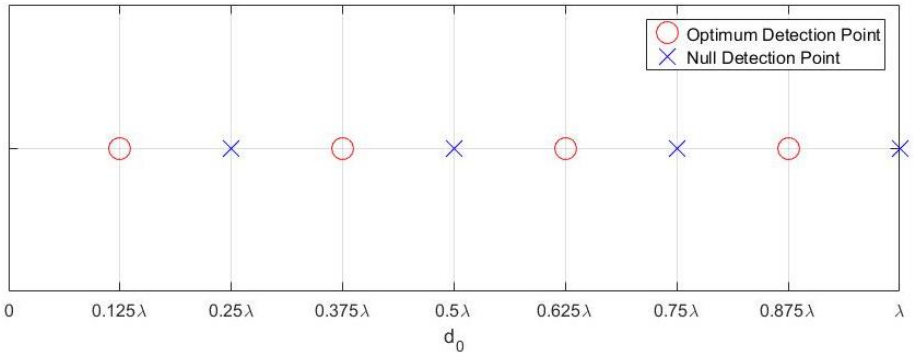

Figure 11 - Distribution of the 'Optimum Detection Point' and of the 'Null Detection Point'

It shall be possible to observe that the points happen him alternatively outdistanced $\frac{\lambda}{8}$.

Based on the above, is possible to numerically analyze, in Matlab® environment, the reconstruction sensibility to the change of the d_0 distance. Implementing the eq. (32) ranging $d_0$from 0 to λ and assuming $\Delta_\theta(t)$ null, it is reasonable to effect the $x(t)$ motion extraction through eq. (37) appraising the technique sensibility through the correspondence verification of the reconstructed motion with the fixed motion.

Particularly, by fixing the eq. (32) parameters to the values shown in Table 1,

Table 1. Fixed parameters for the elaboration

f_0	1 GHz
λ	0.30 m
L	1
d_0	$0 - \lambda$
$\Delta\theta(t)$	0

to the purpose to carry out such analysis, it is likely to impose for the intercepted object an oscillatory motion analytically described by eq. (43)

$$x(t) = A_m \sin(2\pi f_m t) \tag{43}$$

with

Table 2. Fixed parameters for the target motion

A_m	1 mm
f_m	1 Hz

where A_m is the motion amplitude and f_m is the oscillation frequency. The choice of the parameters shown in Table 2 is not casual. The A_m motion amplitude, in fact, is such to be respected the condition expressed in eq. (44), necessary to be able to employ the 'Small Angle Approximation.'

$$|x(t)| \ll \lambda \tag{44}$$

The f_m oscillation frequency, instead, is slow oscillatory motions characteristic as some important human physiological phenomena, for example, the respiration and the heart beats.

Figure 12 shows the $x(t)$ oscillation amplitude values, detected by varying the d_0 distance, through the FFT signal spectrum analysis.

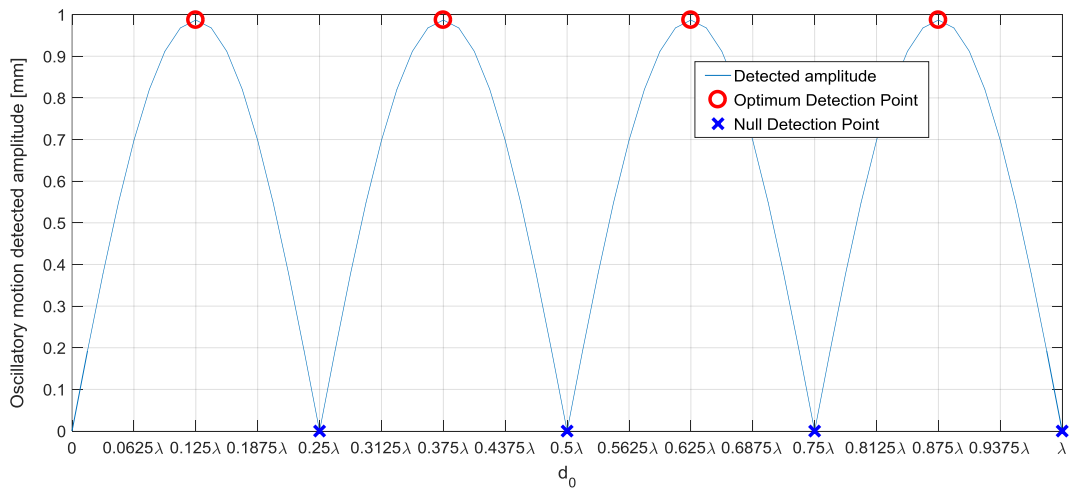

Figure 12 - Oscillatory motion detected amplitude by varying the distance changing

As can be seen, in correspondence of the 'Optimum Detection Point', the detected amplitudes are conforming to the fixed one (Table 2 - $A_m = 1mm$), showing that, with the target placed to these distances, is possible to effect some reliable reconstructions. In correspondence of the 'Null Detection Point', instead, the oscillatory motion detected amplitudes are null, underlining, therefore, the unreliability of the reconstruction when the objective is placed to these distances.

From these data, by the comparison between the obtained values and the exprected ones, the technique sensibility can be analyzed depending on the d_0 distance considering the percentage error committed. Figure 13 show this analysis result.

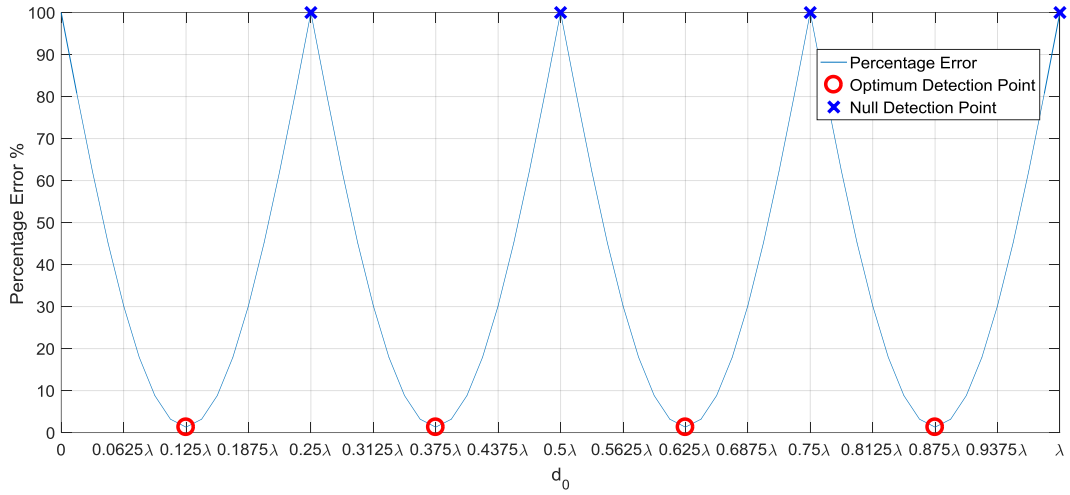

Figure 13 - Reconstruction percentage error depending on the distance

The error appears null in the 'Optimum Detection Point' correspondence, while it is resulting maximum in the 'Null Detection Point' correspondence. To intermediary distances, the error decreases or it increases approaching or leaving from 'Optimum Detection Point' causing, in these cases, a distortion of the detected ampleness.

Finally, as can be seen from eq. (37), a further aleration element in the motion reconstruction is introduced by the L factor, used for modeling in simplified way the propagation losses. This factor, previously discussed in summary way, actually includes different phenomena, such as the propagation losses, those introduced at different stages, by circuitry, and those due to the backscattered capabilities, of the intercepted objects. All these phenomena have varying dynamics related to the environmental conditions such as temperature and humidity. These factor fluctuations make, therefore this type of the reconstruction exposed to further and unpredictable oscillations.

3. IQ Signals Modulation and Demodulation in Doppler Radar CW

The classical Doppler elaboration, in the CW radars, based on the transmitted and received signal beat and on the following product filtering to the purpose to extract the backscattered signal phase, modulated by the target movement, has some difficulties. Particularly, as referred to above, exist some distances from the radar

to the target, known as 'Null Detection Point', from which, with this approach, may be no correct extraction of the object of interest phase.

An alternative approach, to resolve this problem, is based on the I/Q modulation use. In Figure 14 and in Figure 15 are given the blocks diagrams of the two main macro-elements to this system realization, so a I/Q modulator and demodulator.

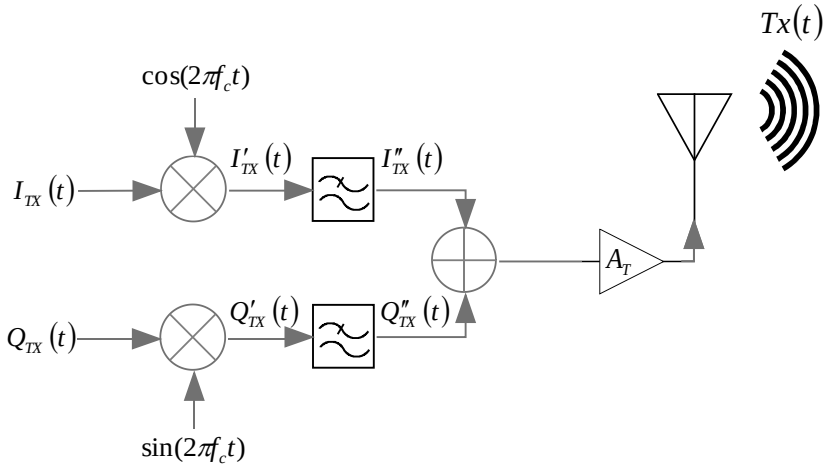

Figure 14 - I/Q modulator architecture

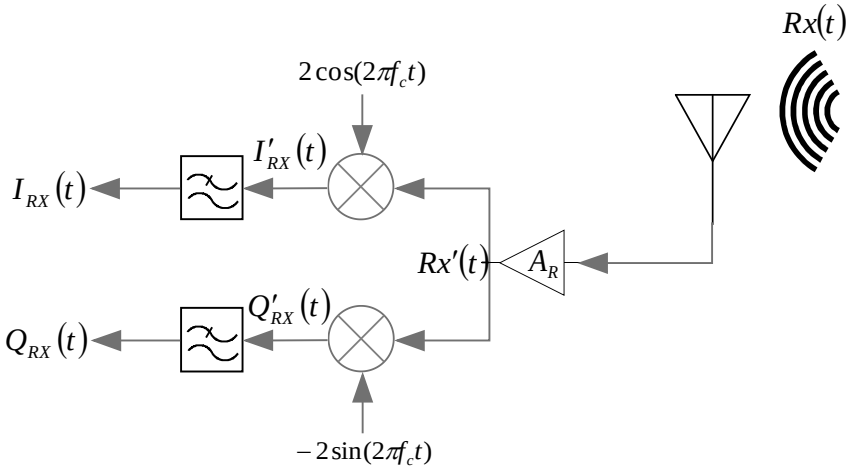

Figure 15 - I/Q demodulator architecture

In Figure 16 are given the typical scenery in which these systems operate.

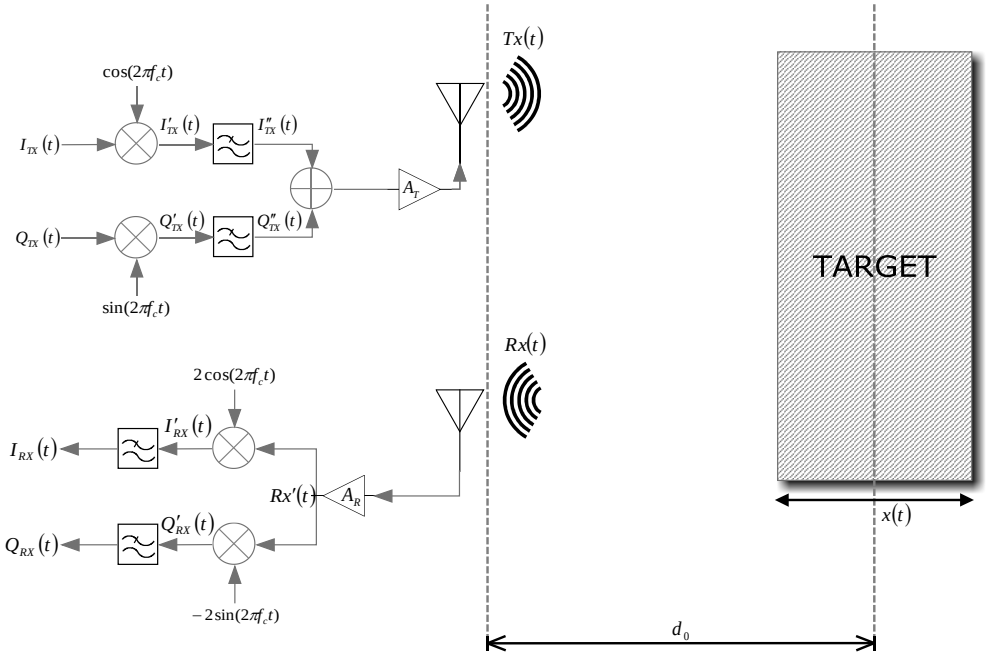

Figure 16 - Typical scenery for the vibrations monitoring applications through a CW radar Doppler.

As in the case previous case, it is possible to define the function that describes the distance from the radar to the target varying the time as shown in the eq. (45) and starting from this, can be obtained the 'Round Trip' time (eq. (46)).

$$\bar{x}(t) = d_0 + x(t) \tag{45}$$

$$\tau(t) = \frac{2\bar{x}(t)}{c} = \frac{2d_0}{c} + \frac{2x(t)}{c} \tag{46}$$

To understand in the detail how this radar type operates, it is necessary to analytically formulate the particular problem. The first operation phase is, of course, the signals generation. Particularly, for this architecture, it is necessary to produce in phase component (I) and in quadrature component (Q) to be transferred to the I/Q modulator as shown above in the Figure 14. Since it is desired to transmit a CW monochrome signal, it is necessary to fix at the I/Q modulator component to the expressions described in the eqs. (47)-(48),

$$I_{TX}(t) = \cos[2\pi f_{\mathrm{IF}} t + \theta_{\mathrm{IF}}(t)] \tag{47}$$

$$Q_{TX}(t) = \sin[2\pi f_{\mathrm{IF}} t + \theta_{\mathrm{IF}}(t)] \tag{48}$$

where f_{IF} named intermediary frequency and $\theta_{IF}(t)$ is the signal generator phase noise. The two signal components, applied to different modulator branches, suffer, in sequence, the mixing and filtering operations, that move their spectrum from the f_{IF} intermediate frequency modulator to the $(f_c - f_{IF})$ carrying frequency. This

operations sequence, shown in Figure 14 and known as 'UP-CONVERSION', is described in detail from the eq. (49) to the eq. (53).

$$\begin{aligned} I'_{TX}(t) &= \cos[2\pi f_c t + \theta_c(t)] \cdot I_{TX}(t) = \\ &= \cos[2\pi f_c t + \theta_c(t)] \cos[2\pi f_{IF} t + \theta_{IF}(t)] = \\ &= \frac{1}{2}\{\cos[2\pi(f_c + f_{IF})t + \theta_c(t) + \theta_{IF}(t)] \\ &+ \cos[2\pi(f_c - f_{IF})t + \theta_c(t) - \theta_{IF}(t)]\} \end{aligned} \tag{49}$$

$$\begin{aligned} Q'_{TX}(t) &= \sin[2\pi f_c t + \theta_c(t)] \cdot Q_{TX}(t) = \\ &= \sin[2\pi f_c t + \theta_c(t)] \sin[2\pi f_{IF} t + \theta_{IF}(t)] = \\ &= \frac{1}{2}\{\cos[2\pi(f_c - f_{IF})t + \theta_c(t) - \theta_{IF}(t)] \\ &- \cos[2\pi(f_c + f_{IF})t + \theta_c(t) + \theta_{IF}(t)]\} \end{aligned} \tag{50}$$

After the low pass filter:

$$I''_{TX}(t) = \frac{1}{2}\cos[2\pi(f_c - f_{IF})t + \theta_{TX}(t)] \tag{51}$$

$$Q''_{TX}(t) = \frac{1}{2}\cos[2\pi(f_c - f_{IF})t + \theta_{TX}(t)] \tag{52}$$

where

$$\theta_{TX}(t) = \theta_c(t) - \theta_{IF}(t) \tag{53}$$

represents the transmitter phase noise, with $\theta_c(t)$ that describes the local oscillator phase noise at f_c frequency.

Before being transmitted, the two signal components, are added and the result is amplified and transferred to ether through an antenna use. This operation result is described by the eq. (54),

$$Tx(t) = A_T[I''_{TX}(t) + Q''_{TX}(t)] = A_T \cos[2\pi(f_c - f_{IF})t + \theta_{TX}(t)] \tag{54}$$

where is the A_T transmission gain.

The received signal, shown in the eq. (55), exhibits the same transmitted signal form, in comparison to which it results however delayed of $\tau(t)$, due to the propagation delay, (eq. (46)) and attenuated by L factor, due to the target 'Radar Cross-Section' and to propagation losses.

$$Rx(t) = L \cdot Tx\big(t - \tau(t)\big) \tag{55}$$

Replacing the eqs. (46) and (54) inside the eq. (55), as shown in the eq. (56), the received signal, after the amplification stadium present in the receiver, is showing as in the eq. (57), where A_R is the receiver gain.

$$\begin{aligned} Rx(t) &= L\,A_T \cos\big[2\pi(f_c - f_{IF})\big(t - \tau(t)\big) + \theta_{TX}\big(t - \tau(t)\big)\big] = \\ &= L\,A_T \cos\left[2\pi(f_c - f_{IF})t - \frac{4\pi(f_c - f_{IF})d_0}{c} - \frac{4\pi(f_c - f_{IF})x(t)}{c}\right. \\ &\left. + \theta_{TX}\left(t - \frac{2d_0}{c}\right)\right] \end{aligned} \tag{56}$$

$$\begin{aligned} Rx'(t) &= \\ &= A_R\,L\,A_T \cos\left[2\pi(f_c - f_{IF})t - \frac{4\pi(f_c - f_{IF})d_0}{c} - \frac{4\pi(f_c - f_{IF})x(t)}{c}\right. \\ &\left. + \theta_{TX}\left(t - \frac{2d_0}{c}\right)\right] \end{aligned} \tag{57}$$

Defining A as shown in the eq. (58), it is possible reformulate the eq. (57) as shown in the eq. (59).

$$A = A_R \cdot L \cdot A_T \tag{58}$$

$$\begin{aligned} Rx'(t) &= \\ &= A \cos\left[2\pi(f_c - f_{IF})t - \frac{4\pi(f_c - f_{IF})d_0}{c} - \frac{4\pi(f_c - f_{IF})x(t)}{c}\right. \\ &\left. + \theta_{TX}\left(t - \frac{2d_0}{c}\right)\right] \end{aligned} \tag{59}$$

At this point, as shown in Figure 15, the received signal is divided and parallelly assigned as input to the two demodulator branches for the I/Q components extraction. The spectrum of the two signal components, through mixing and filtering operations, is once again moved from $(f_c - f_{IF})$ carrying frequency to the f_{IF} intermediate frequency. This operations sequence, shown in Figure 15 and known as 'DOWN-CONVERSION', it is described in detail from the eq. (60) to the eq. (63).

$$
\begin{aligned}
I'_{RX}(t) &= Rx'(t)2\cos[2\pi f_c t + \theta_c(t)] = \\
&= A\cos\left[2\pi(f_c - f_{IF})t - \frac{4\pi(f_c - f_{IF})d_0}{c} - \frac{4\pi(f_c - f_{IF})x(t)}{c}\right. \\
&\left. + \theta_{TX}\left(t - \frac{2d_0}{c}\right) + 2\pi f_c t + \theta_c(t)\right] \\
&+ A\cos\left[2\pi(f_c - f_{IF})t - \frac{4\pi(f_c - f_{IF})d_0}{c} - \frac{4\pi(f_c - f_{IF})x(t)}{c}\right. \\
&\left. + \theta_{TX}\left(t - \frac{2d_0}{c}\right) - 2\pi f_c t - \theta_c(t)\right] = \\
&= A\cos\left[2\pi(2f_c - f_{IF})t - \frac{4\pi(f_c - f_{IF})d_0}{c} - \frac{4\pi(f_c - f_{IF})x(t)}{c}\right. \\
&\left. + \theta_{TX}\left(t - \frac{2d_0}{c}\right) + \theta_c(t)\right] \\
&+ A\cos\left[-2\pi f_{IF}t - \frac{4\pi(f_c - f_{IF})d_0}{c} - \frac{4\pi(f_c - f_{IF})x(t)}{c}\right. \\
&\left. + \theta_{TX}\left(t - \frac{2d_0}{c}\right) - \theta_c(t)\right]
\end{aligned}
\tag{60}
$$

$$
\begin{aligned}
Q'_{RX}(t) &= Rx'(t)\,2\sin[2\pi f_c t + \theta_c(t)] = \\
&= A\sin\left[2\pi(f_c - f_{IF})t - \frac{4\pi(f_c - f_{IF})d_0}{c} - \frac{4\pi(f_c - f_{IF})x(t)}{c}\right. \\
&\left. + \theta_{TX}\left(t - \frac{2d_0}{c}\right) + 2\pi f_c t + \theta_c(t)\right] \\
&+ A\sin\left[2\pi(f_c - f_{IF})t - \frac{4\pi(f_c - f_{IF})d_0}{c} - \frac{4\pi(f_c - f_{IF})x(t)}{c}\right. \\
&\left. + \theta_{TX}\left(t - \frac{2d_0}{c}\right) - 2\pi f_c t - \theta_c(t)\right] = \\
&= A\sin\left[2\pi(2f_c - f_{IF})t - \frac{4\pi(f_c - f_{IF})d_0}{c} - \frac{4\pi(f_c - f_{IF})x(t)}{c}\right. \\
&\left. + \theta_{TX}\left(t - \frac{2d_0}{c}\right) + \theta_c(t)\right] \\
&+ A\sin\left[-2\pi f_{IF}t - \frac{4\pi(f_c - f_{IF})d_0}{c} - \frac{4\pi(f_c - f_{IF})x(t)}{c}\right. \\
&\left. + \theta_{TX}\left(t - \frac{2d_0}{c}\right) - \theta_c(t)\right]
\end{aligned}
\tag{61}
$$

After the low pass filter:

$$I_{RX}(t) = \\ = A\cos\left[-2\pi f_{IF}t - \frac{4\pi(f_c - f_{IF})d_0}{c} - \frac{4\pi(f_c - f_{IF})x(t)}{c} \\ + \theta_{TX}\left(t - \frac{2d_0}{c}\right) - \theta_c(t)\right] \tag{62}$$

$$Q_{RX}(t) = \\ = A\sin\left[-2\pi f_{IF}t - \frac{4\pi(f_c - f_{IF})d_0}{c} - \frac{4\pi(f_c - f_{IF})x(t)}{c} \\ + \theta_{TX}\left(t - \frac{2d_0}{c}\right) - \theta_c(t)\right] \tag{63}$$

It is possible reformulate these expressions, in compact form, as shown in the eqs. (64) and (65)

$$I_{RX}(t) = A\cos\left[-\alpha - \beta - \gamma + \theta_{TX}\left(t - \frac{2d_0}{c}\right) - \theta_c(t)\right] \tag{64}$$

$$Q_{RX}(t) = A\sin\left[-\alpha - \beta - \gamma + \theta_{TX}\left(t - \frac{2d_0}{c}\right) - \theta_c(t)\right] \tag{65}$$

effecting the substitutions indicated in the eqs. (66)-(68).

$$\alpha = 2\pi f_{IF}t \tag{66}$$

$$\beta = \frac{4\pi(f_c - f_{IF})d_0}{c} \tag{67}$$

$$\gamma = \frac{4\pi(f_c - f_{IF})x(t)}{c} \tag{68}$$

Using the equation (66) is possible reformulate the eqs. (47) and (48) as shown following.

$$I_{TX}(t) = \cos[\alpha + \theta_{IF}(t)] \tag{69}$$

$$Q_{TX}(t) = \sin[\alpha + \theta_{IF}(t)] \tag{70}$$

Through the transmitted (eqs. (69) and (70)) and received (Equations (64) and (65)) I/Q component elaboration, according to the scheme shown in Figure 17, it is possible to extract the signal received phase containing the information on the monitored target motion.

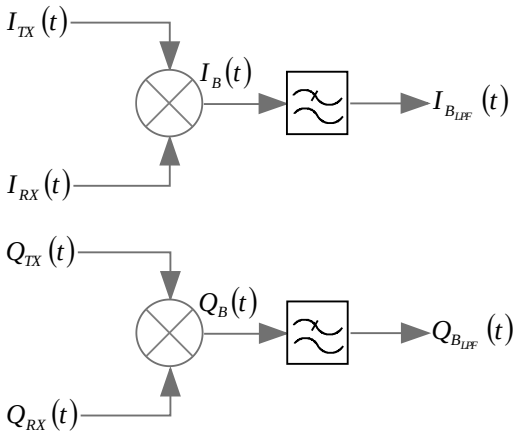

Figure 17 - I/Q component elaboration for the phase extraction

The operations sequence, shown in Figure 17, is described from the eqs. (71)-(77).

$$\begin{aligned} I_B(t) &= I_{TX}(t) \cdot I_{RX}(t) = \\ &= \frac{A}{2}\cos\left\{-\beta-\gamma+\theta_{TX}\left(t-\frac{2d_0}{c}\right)-[\theta_c(t)-\theta_{IF}(t)]\right\} \\ &+ \frac{A}{2}\cos\left\{-2\alpha-\beta-\gamma+\theta_{TX}\left(t-\frac{2d_0}{c}\right)-[\theta_c(t)+\theta_{IF}(t)]\right\} \end{aligned} \tag{71}$$

$$\begin{aligned} Q_B(t) &= Q_{TX}(t) \cdot Q_{RX}(t) = \\ &= \frac{A}{2}\sin\left\{-\beta-\gamma+\theta_{TX}\left(t-\frac{2d_0}{c}\right)-[\theta_c(t)-\theta_{IF}(t)]\right\} \\ &+ \frac{A}{2}\sin\left\{-2\alpha-\beta-\gamma+\theta_{TX}\left(t-\frac{2d_0}{c}\right)-[\theta_c(t)+\theta_{IF}(t)]\right\} \end{aligned} \tag{72}$$

After the low pass filter, by the substitution shown in the eq. (53):

$$I_{B_{LPF}}(t) = \frac{A}{2}\cos\left[-\beta-\gamma+\theta_{TX}\left(t-\frac{2d_0}{c}\right)-\theta_{TX}(t)\right] \tag{73}$$

$$Q_{B_{LPF}}(t) = \frac{A}{2}\sin\left[-\beta-\gamma+\theta_{TX}\left(t-\frac{2d_0}{c}\right)-\theta_{TX}(t)\right] \tag{74}$$

replacing in the eqs. (73) and (74) the eqs. (67) and (68) and defining

$$\Delta\theta_{TX}(t) = \theta_{TX}\left(t-\frac{2d_0}{c}\right)-\theta_{TX}(t) \tag{75}$$

the eqs. (76) and (77) are obtained.

$$I_{B_{LPF}}(t) = \frac{A}{2}\cos\left[-\frac{4\pi(f_c - f_{IF})d_0}{c} - \frac{4\pi(f_c - f_{IF})x(t)}{c} + \Delta\theta_{TX}(t)\right] \quad (76)$$

$$Q_{B_{LPF}}(t) = \frac{A}{2}\sin\left[-\frac{4\pi(f_c - f_{IF})d_0}{c} - \frac{4\pi(f_c - f_{IF})x(t)}{c} + \Delta\theta_{TX}(t)\right] \quad (77)$$

These last two signals represent in phase and in quadrature component used for the phase extraction and therefore for the target oscillatory motion reconstruction, in accord with the geometric representation in the Cartesian complex plane illustrated in Figure 18.

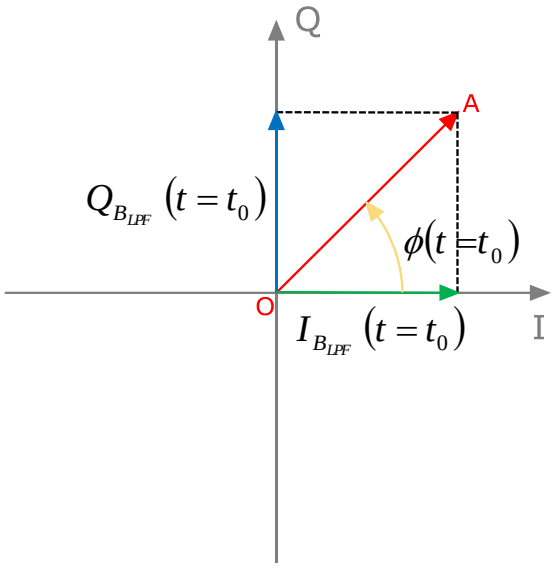

Figure 18 - I/Q component representation in the complex plane

The $\overrightarrow{OA}$ vector, represented in red in Figure 18 to a generic $t = t_0$ time instant, are described by the eq. (78).

$$\overrightarrow{OA} = I_{B_{LPF}}(t) + j\, Q_{B_{LPF}}(t) \quad (78)$$

It is possible to express the vector amplitude as indicated in the eq. (79)

$$|\overrightarrow{OA}| = \sqrt{\left[I_{B_{LPF}}(t)\right]^2 + \left[Q_{B_{LPF}}(t)\right]^2} = \frac{A}{2} \quad (79)$$

and besides

$$\tan[\phi(t)] = \frac{Q_{B_{LPF}}(t)}{I_{B_{LPF}}(t)} \quad (80)$$

where $\phi(t)$ indicates the phase to extract and its expression is shown in the equation (81).

$$\phi(t) = \left[-\beta - \gamma + \Delta_{\theta_{TX}}(t)\right] = \\ = \left[-\frac{4\pi(f_c - f_{IF})d_0}{c} - \frac{4\pi(f_c - f_{IF})x(t)}{c} + \Delta\theta_{TX}(t)\right] \quad (81)$$

Assuming $\Delta\theta_{TX}(t)$ null the eq. (82),

$$\arctan\left[\frac{Q_{B_{LPF}}(t)}{I_{B_{LPF}}(t)}\right] = \left[-\frac{4\pi(f_c - f_{IF})d_0}{c} - \frac{4\pi(f_c - f_{IF})x(t)}{c}\right] \quad (82)$$

from which is easily isolate the $\bar{x}(t)$ function (eq. (45)) as shown in eq. (83).

$$\bar{x}(t) = d_0 + x(t) = -\arctan\left[\frac{Q_{B_{LPF}}(t)}{I_{B_{LPF}}(t)}\right]\frac{c}{4\pi(f_c - f_{IF})} \quad (83)$$

Figure 19 gives an exhaustive geometric representation, in the Cartesian complex plan, to a generic d_0 distance, of the problem analytically described.

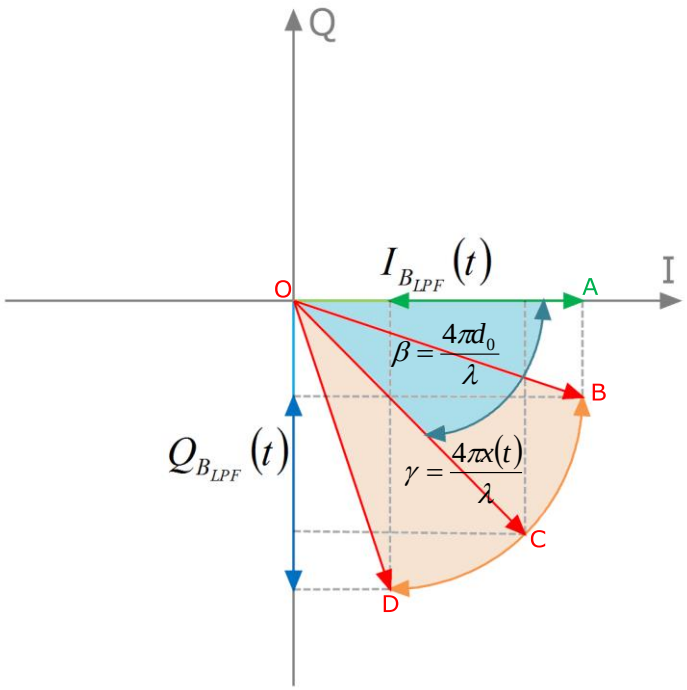

Figure 19 - β (eq. (67)) and γ (eq. (68)) representation on the complex plane

The $\overrightarrow{OC}$ vector represents the eqs. (76) and (77) considering only the β phase term that has not time dependence. The $\overrightarrow{OC}$ vector rotates inside the area individualized from the $\overrightarrow{OB}$ and $\overrightarrow{OD}$ vectors as a consequence of the γ phase term that introducing time dependency because is linearly related to the $x(t)$ motion.

The eq. (83), and even more the geometric representation (Figure 19), immediately put in prominence as, unlike the preceding case, the phase extraction is not subject

to the different factors, which the losses (L) and gains (A), and to their fluctuations, that intervene only in the amplitude expression (eq. (79)).

In the hypothesis that in the $[t_0, t_1]$ acquisition interval the middle value is null, it is possible finally to reconstruct the target motion as shown in the eq. (84).

$$x(t) = \bar{x}(t) - \frac{1}{t_1 - t_0} \int_{t_0}^{t_1} \bar{x}\,(t)dt \qquad t \in [t_0, t_1] \tag{84}$$

Likewise to how much effected in precedence in the Doppler elaboration in the classical CW radar systems case, is possible to numerically analyze, in Matlab® environment, the reconstruction sensibility at d_0 distance varying. Implementing the expressions of the eqs. (76) and (77) for d_0 values between 0 and λ and assuming $\Delta\theta_{TX}(t)$ null, it is reasonable to effect the $x(t)$ motion extraction through the eq. (84) appraising the technique sensibility through the verification of the correspondence between the reconstructed motion and the fixed motion.

Particularly, as in the preceding case, the eqs. (76) and (77) parameters have been fixed to shown values in Table 3 and the oscillatory motion of the intercepted object has analytically been described by the eq. (43).

Table 3. Fixed parameters for I/Q elaboration

f_c	1 GHz
f_{IF}	1 kHz
λ	0.30 m
L	1
d_0	$0 - \lambda$
$\Delta\theta_{TX}(t)$	0

In conformity with, the Figure 19, Figure 20 shows the elaborate signals representation in the complex plan at d_0 distance varying. It is clear that, the vector having eqs. (76) and (77) as component, is rotating clockwise at d_0 distance varying, realizing a complete turn with a $\frac{\lambda}{2}$ spatial period. The presence of this periodicity produces, evidently, an ambiguity in the d_0 distance extraction.

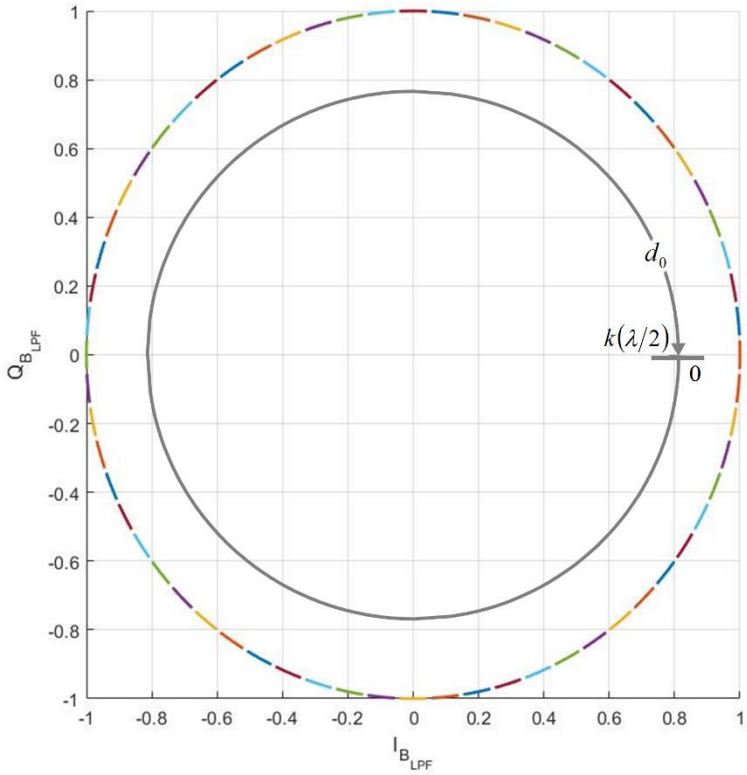

Figure 20 - I/Q component representation in the complex plane at d_0 distance varying

The Figure 21 shows the detected amplitude values of the $x(t)$ oscillation at f_m frequency, related at d_0 distance varying, obtained through FFT spectral analysis.

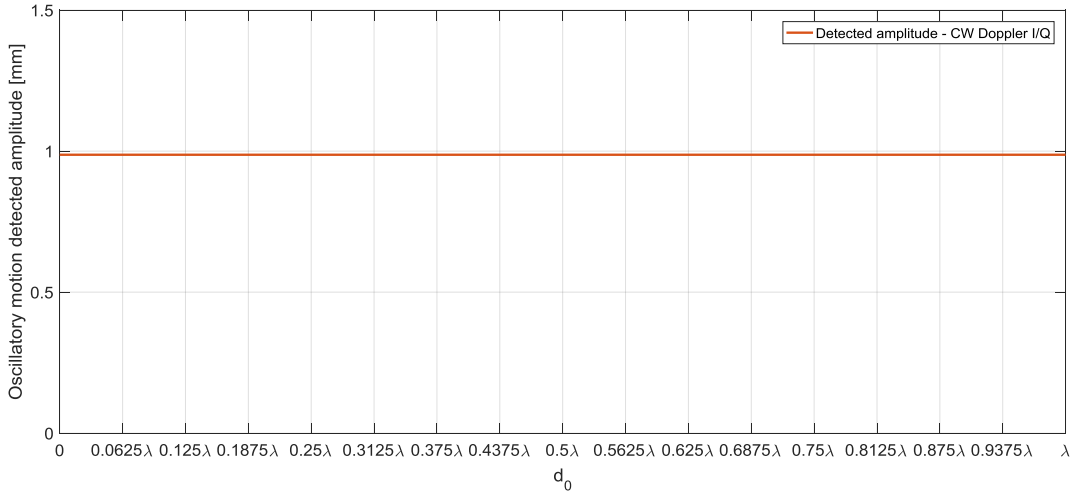

Figure 21 – Oscillating motion detected amplitudes, with I/Q signal modulation at distance varying

The detected amplitudes, unlike the results obtained in classical CW Doppler elaboration, (Figure 12), are in line with the fixed (Table 2 - $A_m = 1mm$) for every d_0 distance value, with consequent percentage error decrease (Figure 22).

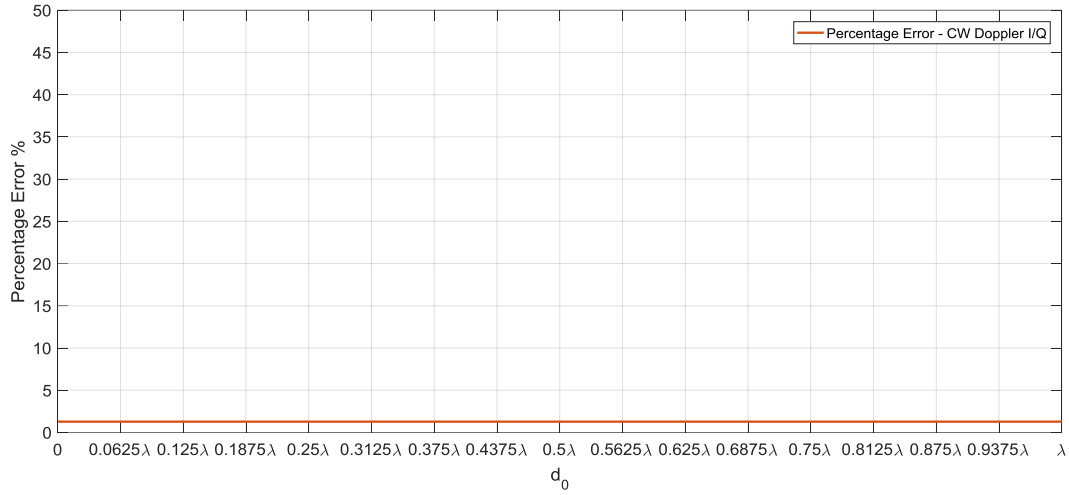

Figure 22 – Reconstruction percentage error, with I/Q signal modulation, at distance varying

In Figure 23 and in Figure 24, the results and the percentage errors obtained, with both solutions, are compared.

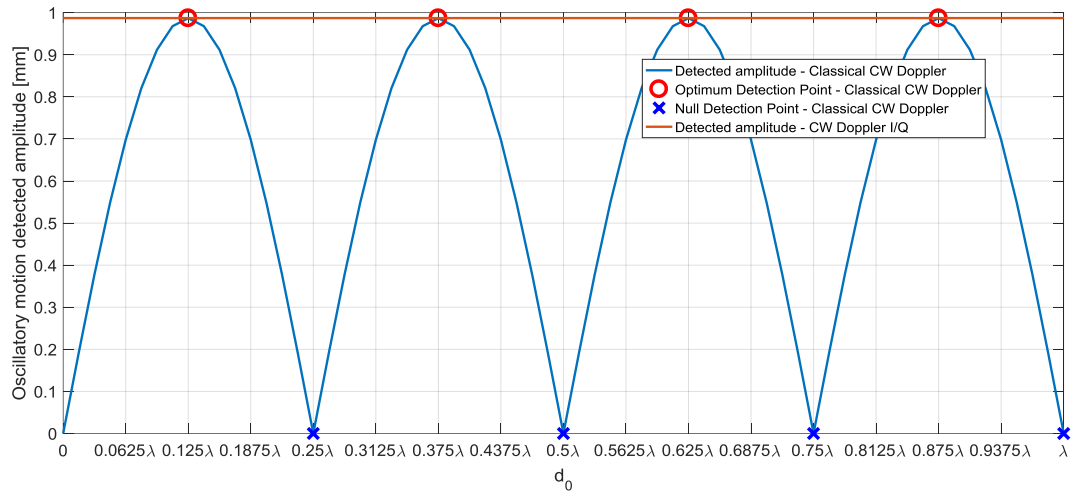

Figure 23 – Oscillating motion detected amplitude. Classical CW Doppler vs I/Q CW Doppler

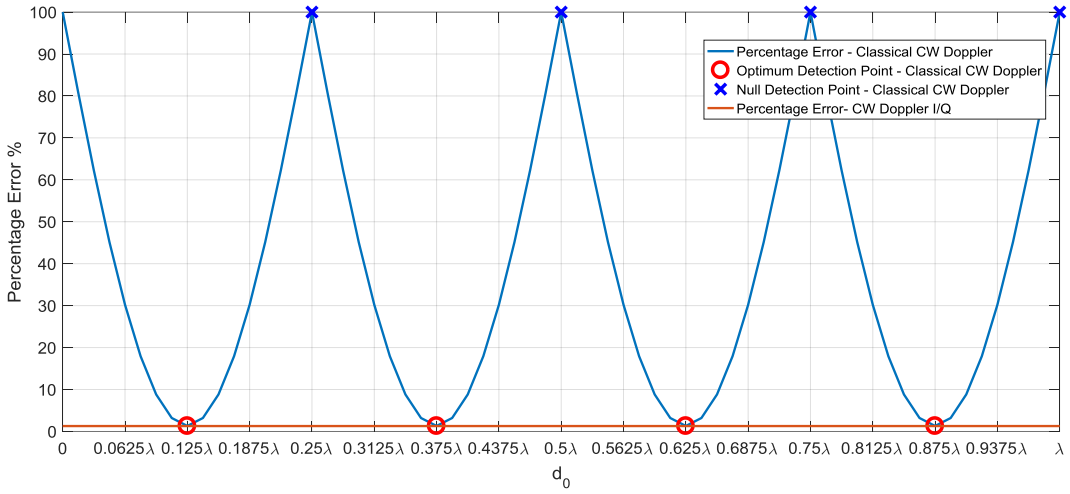

Figure 24 – Reconstruction percentage error. Classical CW Doppler vs I/Q CW Doppler

From the results comparison, obtained through the two types of explored and exposed approaches, it appears evident as, in the CW radars based on the classical Doppler elaboration, the critical issues resulting from the 'Null Detection Point' presence, in terms of annulment and distortion of the detected oscillation amplitudes, may adequately be exceeded through the I/Q signals modulation.

Software Defined Doppler Radar for vibrations monitoring

A Doppler elaboration based on a Software Defined Radar (SDRadar) system is proposed in this work as alternative to standard hardware architectures for vibrations detection. An SDRadar prototype, fully realized by software, is implemented to satisfy various frequency detection requirements, even in the presence of slow and small oscillations, by simply changing 'real time' the useful parameters (e.g. bandwidth and acquisition time). Particularly, thanks to the elevated flexibility guaranteed by the Software-Defined approach, it has been possible to integrate into the same platform, and therefore using the same hardware, both the elaboration methodologies previously analyzed, Classical CW Doppler Radar and IQ CW Doppler Radar, in order to decrease the faults. Experimental validations by a device able to produce a harmonic motion, are discussed to prove the proper detection capabilities of the proposed architecture.

1. Hardware requirements and devices used

The main purpose of the proposed approach, detailed above, consists in the alternative, flexible and economic platform implementation, for the detection of vibrations and physiological parameters interpretable as such. The hardware and devices choice has been, therefore, opportunely aimed to satisfy such requisite. From this point of view, the SDRadar system architecture is extremely essential, particularly, as represented in Figure 25, the platform consists of four main macroblocks:

- General Purpose PC able to support LabView and equipped with an Ethernet connection.
- NI USRP -2920 SDR transceiver.
- A standard vertical dipole antenna in transmission.
- An antenna, model A0303, produced by Impinj which has a strong near field.

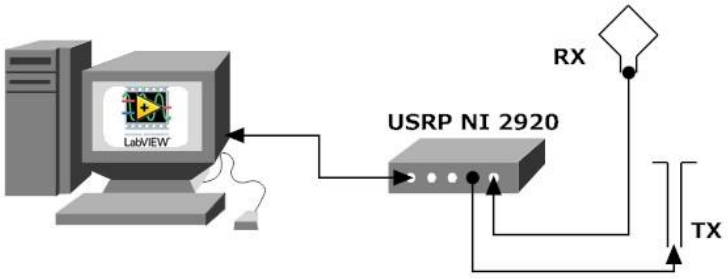

Figure 25 - Software Defined Doppler Radar. Hardware macroblocks

The PC is connected to the SDR transceiver through the Ethernet interface. The radiant elements connection to the transceiver is realized instead through coaxial cables with SMA connector.

1.1. General Purpose PC

A particularly advantageous aspect of the radar platform implemented, and more generally of the radio systems in Software Defined technology, is represented by the absolute independence from ad hoc elaboration modules. All signals processing operations, from the generation to the filtering and computer graphics visualization, are carried out, in fact, through LabView software modules in execution on a General Purpose PC (Figure 26).

Figure 26 - Standard General Purpose PC

The minimum requirements of this PC, both from the hardware point of view that from the software point of view, dictated especially by the necessity to run LabView application in real time, are modest:

- a LabView version that supports SDR devices;
- a general-purpose operating system supported by LabView;
- an Ethernet gigabit interface for the PC to the SDR transceiver connection, to which it transfers the generated signals to transmit and from which draws the signals picked up by the receiver;
- a 32 or 64-bit processor, Pentium IV or later;
- at least 1 GB of RAM.

The possibility to use more performant PC, of course, would allow a more fluid execution of the software modules, improved interaction with the user and reduced execution times, without, however, to extend the system functionalities. Hardware and software of the PC used are summarized in Table 4.

Table 4 - HW and SW of the PC used

Software		
LabView	**O.S.**	
v 14.0.1 Decembers 2014	Windows 7	
Hardware		
Ethernet	**Processor**	**RAM**
Gigabit Ethernet	Intel core i3-4160	12 GB

1.2. SDR NI USRP-2920

The NI USRP-2920 transceiver, shown in Figure 27, belongs to the National Instruments SDR devices family and it is ideal, in combining with LabView software modules, to configure RF systems in short timeframe, due to the lack of ad hoc hardware whose development can ask for rather long times.

Figure 27 - NI USRP-2920 transceiver

The model used does not belong to the top models, limiting mainly the choice of work frequency and bandwidth. The USRP-2920 can work in a frequency range from 50 MHz to 2.2 GHz with 20 MHz bandwidth and it has two physical channels, one usable in transmission/receipt, the other one usable only in receipt. The SDR transceiver is equipped with an IQ modulator and demodulator, respectively placed on the TX channel and on the RX channel.

The device simplified block diagram has shown in the Figure 28.

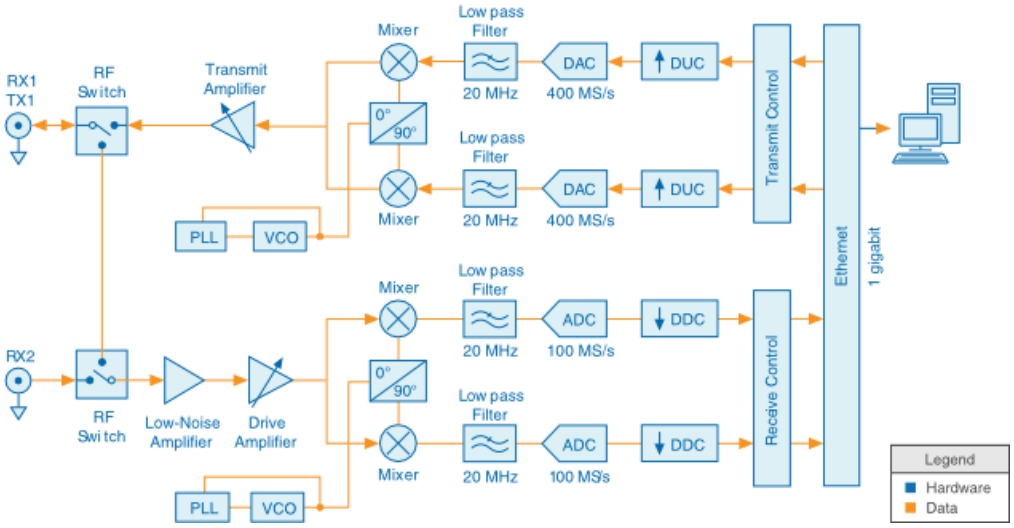

Figure 28 - USRP-2920 block diagram (courtesy of [53])

Despite the limitations on the work frequencies choice, the presence in the architecture of two oscillators including a Phase-Locked Loop (PLL) (Figure 29) represents a great advantage for the Doppler elaborations previously described (eqs. (32) and (81)) because, as discussed extensively in [51-52], it allows to neglect the residual phase noise.

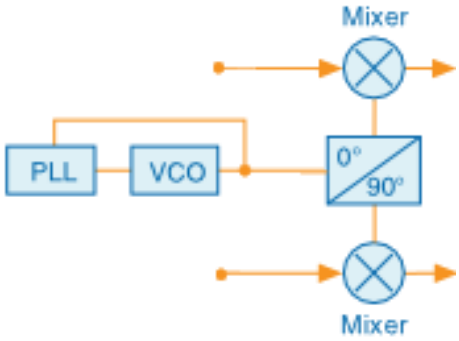

Figure 29 - Oscillator including PLL (courtesy of [53])

1.3. Vertical dipole antenna

The radiant element used in transmission is a vertical dipole antenna, provided with the USRP-2920 by NI, and it is shown in Figure 30.

Figure 30 - Vertical dipole antenna

This type of antenna has an omnidirectional radiation diagram, namely that it doesn't possess a preferential direction in the electromagnetic energy irradiation. A typical example of omnidirectional radiation diagram has shown in Figure 31.

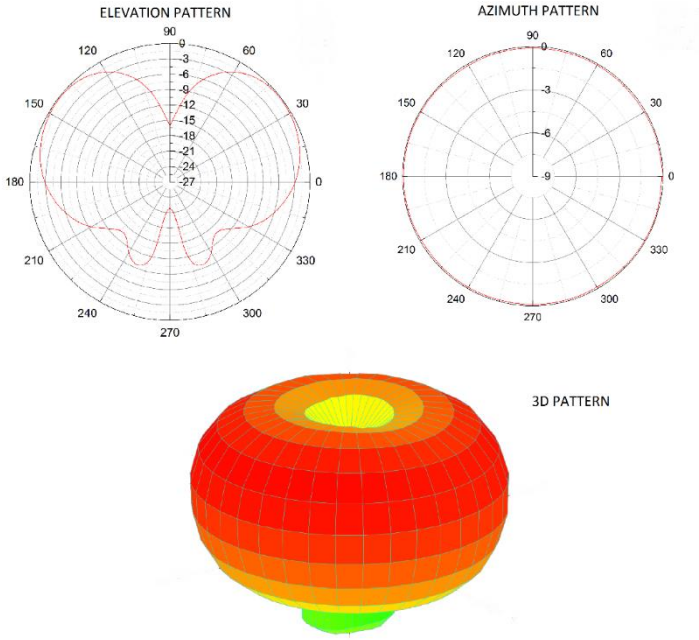

Figure 31 - Typical omnidirectional radiation diagram

The antenna characteristics, in terms of radiation diagram, have allowed using this element as the transmission antenna. Imagining, in fact, a two or more objects monitored (USRP-2920 has only two channels in receipt), it is possible the use of an only omnidirectional antenna in transmission, capable therefore of reaching all targets, and various directional antennas placed in proximity of every target (Figure 32).

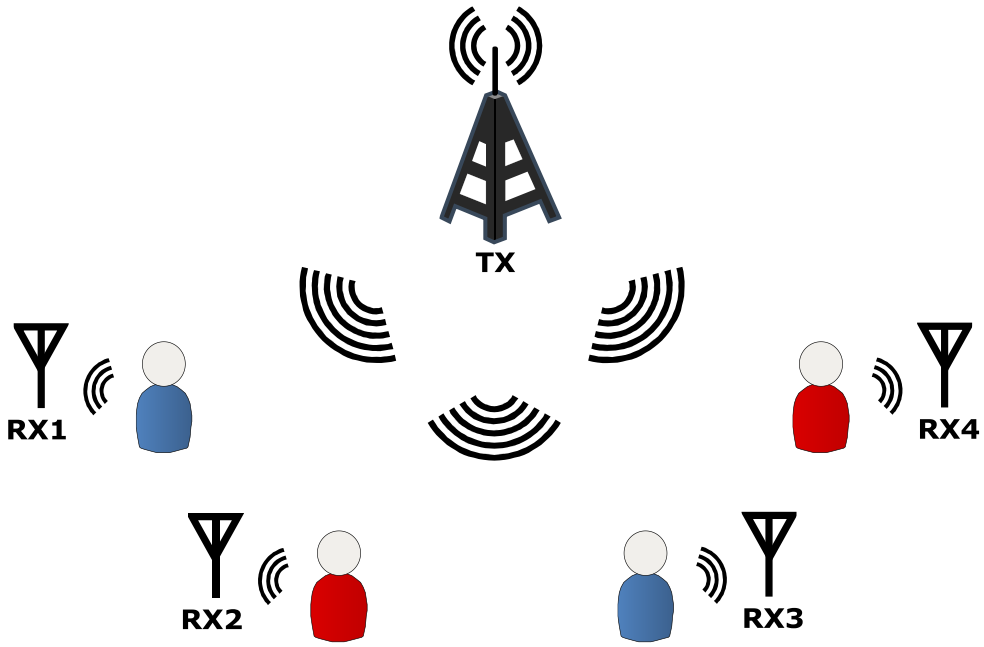

Figure 32 - TX and RX antenna disposition inside the scenario

1.4. Impinj A0303 antenna

For the assumptions made earlier, the antenna used in receipt needs particular specifications. Particularly, in the hypothesis of a scenario where the different monitored objects are illuminated by an only one omnidirectional antenna, it is necessary to place different directional antennas in receipt in the proximities of every target to be able to distinguish, or to select, the different movement sources. Furthermore, this type of organizations allows isolating the environmental noises produced from motion sources present in the environment that aren't investigation object. To this purpose, the A0303 antenna, produced by Impinj and shown in Figure 33, has been used.

Figure 33 - Impinj A0303 (courtesy of [54])

The selected antenna is characterized by compact dimensions (133.4mm x 69.9mm x 19.1 mm), low weight (114 g) and especially by very good performances in near field (Figure 34).

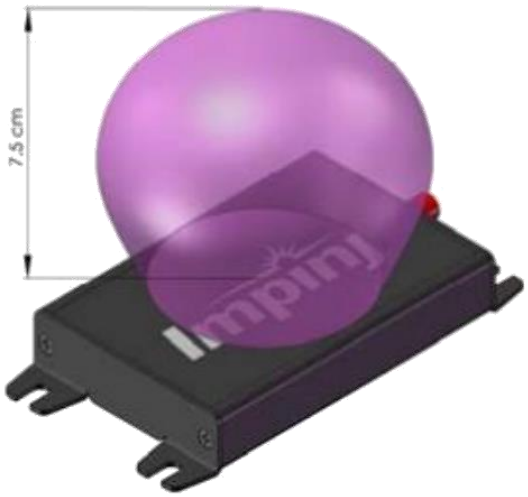

Figure 34 - Impinj A0303. Near-field (courtesy of [54])

Particularly, as shown in the figure above, the antenna used in receipt offers good performances at a range less than 7.5 cm.

1.5. Working frequency choice

The CW Doppler radars have among the principal advantages, the extremely narrow band, due to the single frequency signals use. It is necessary, nevertheless, to choose carefully the SDRadar platform working frequency. The select frequency,

in fact, should be within the antennas and the transceiver bandwidth to guarantee to the system a correct operation.

As regards the transceiver bandwidth, this is known and it is from 50 MHz to 2.2 GHz. For the radiant elements most opportune working frequency choice, instead, has been necessary to measure the two antennas Return Loss through the Vector Network Analyzer Anritsu MS4647A use (Figure 35).

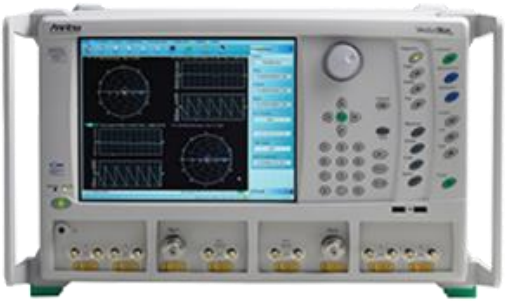

Figure 35 - Anritsu MS4647A VNA

Particularly the S11 scattering parameter magnitude has been pulled out from measurements for the two different antennas in the range 500 MHz. 2.2 GHz. Subsequently, the two measures have been compared as illustrated in Figure 36.

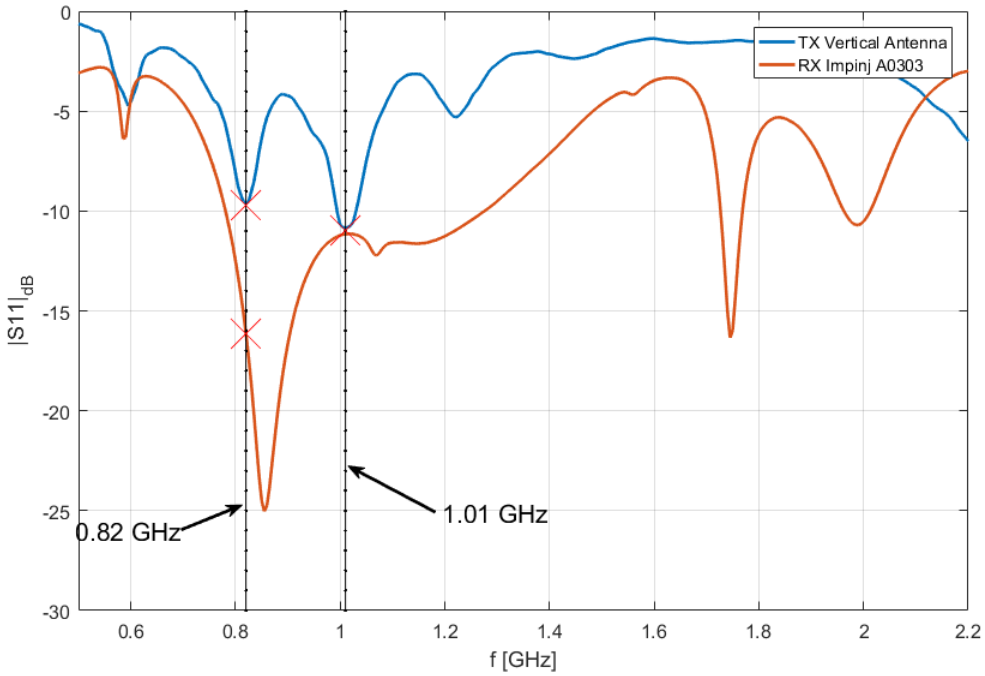

Figure 36 - Return Loss. TX Antenna vs RX Antenna

From the two antennas measurements comparison, imposing as good matching condition, and therefore of the antennas proper operation, a Return Loss value smaller or equal to -10 dB, there are two working frequencies, as summarized in the Table 5.

Table 5 - Return Loss. TX Antenna vs RX Antenna

	0.82 GHz	1.01 GHz
TX Vertical antenna	-9.648 dB	-10.85 dB
RX Impinj A0303	-16.15 dB	-11.16 dB

To the first working frequency, 0.82 GHz, the transmission antenna Return Loss amounts to a little over -10 dB, nevertheless considered sufficient to the system operation because of the receipt antenna good matching. To the second working frequency, 1.01 GHz, the values are more balanced and both are attested just below -10 dB. The SDR transceiver flexibility will allow using both the frequencies, with the possibility to change them in real time according to the necessities.

2. Software architecture

In the SDRadar platform implementation, after having defined the hardware side, it is necessary to carefully design the software side. In this type of systems, which has already been referred to many times, most of the basic operations are realized through LabView software modules in execution on the general purpose PC interfaced with the SDR hardware via Ethernet. To this purpose, it is necessary to understand well the boundary between hardware and software. The SDR transceiver exposes to the software, as represented in Figure 37, four stack of memory, two for writing, containing respectively the I and Q components 16 bits samples to be transferred to the modulator for the transmission and two for reading, containing the I and Q components 16 bits samples processed by the demodulator and coming from the receiver. Besides the hardware shows the software six registers for writing, destined to respectively contain the gain, the carrying frequency and the sampling frequency of the I and Q signals in transmission and in receipt.

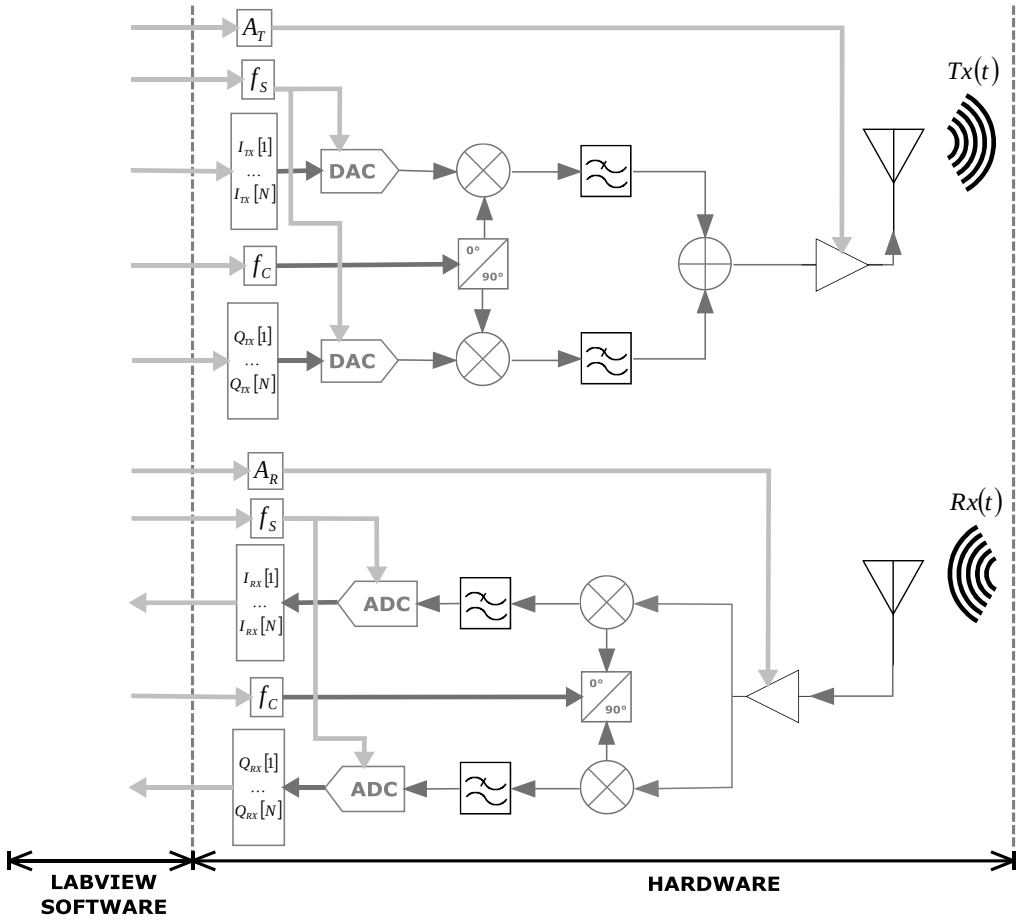

Figure 37 - SDRadar HW and SW

So in light of this, it is possible therefore to conclude that all the operations, excluded UPCONVERSION and DOWNCONVERSION, must be implemented through software modules which require specific design in LabView environment.

The software side must be carefully designed in LabView in order to exactly reproduce the elaboration scheme described in the preceding chapter. The block diagram shown in Figure 38 reproduces the modular architecture realized in LabView.

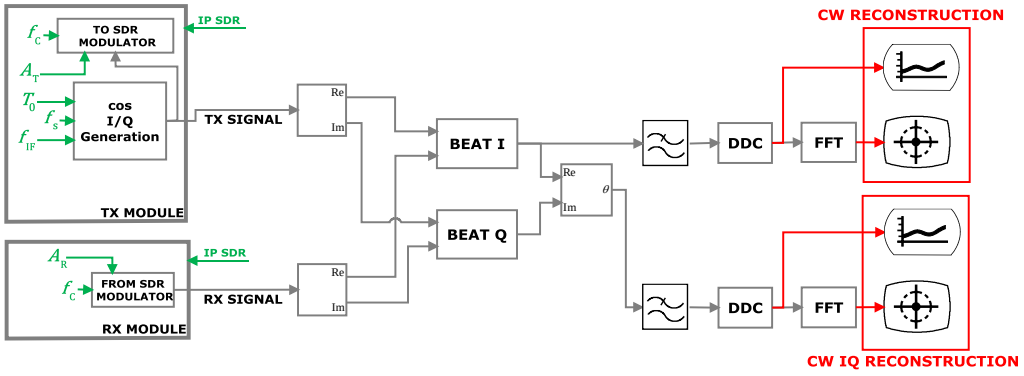

Figure 38 - Software architecture

The block diagram reproduces the signals elaboration flow, in conformity with the theory exposed in precedence, in order to properly reconstruct the monitored objects oscillatory motion. The software side has, besides, a user interface that allows the operator to set the parameters for the signals generation that determines the radar characteristics in terms of resolution, offering besides the possibility to change such parameters also in real time. In Figure 38, the parameters in green are given in input by the user interface while the elaborations results shown to the operator through the same interface are indicated in red.

2.1. User interface

The user interface is presented as shown in Figure 39.

Figure 39 - User interface main part

The section shown in Figure 40 is related to the parameters configurable from the operator and show the obtainable resolutions, in terms of frequency and speed, with these parameters.

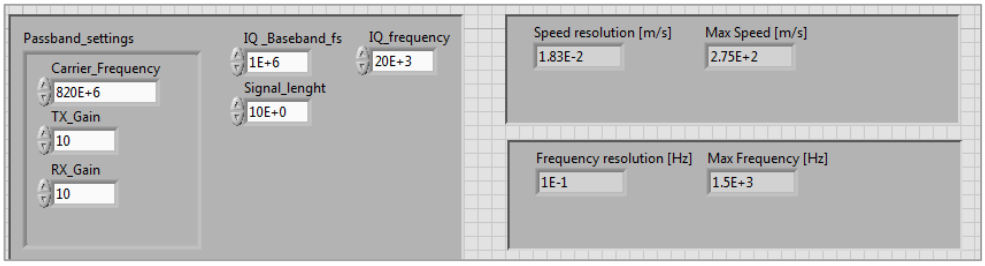

Figure 40 - Input parameters and evalueted achievable resolution

The interface inferior part shows the I and Q transmitted and received components (Figure 41).

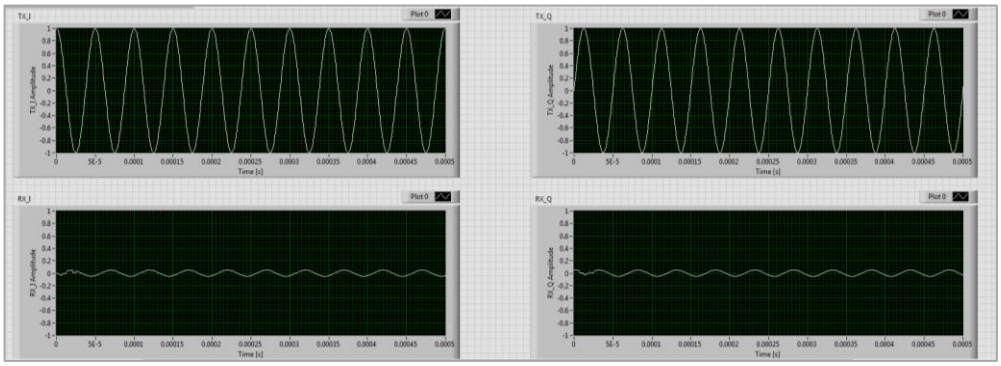

Figure 41 - I and Q transmitted and received components

In the last window section (Figure 42), instead, are shown the vibrations detected, in the time domain and in the frequency domain, on the left using the classical CW elaboration and on the right using the IQ CW elaboration.

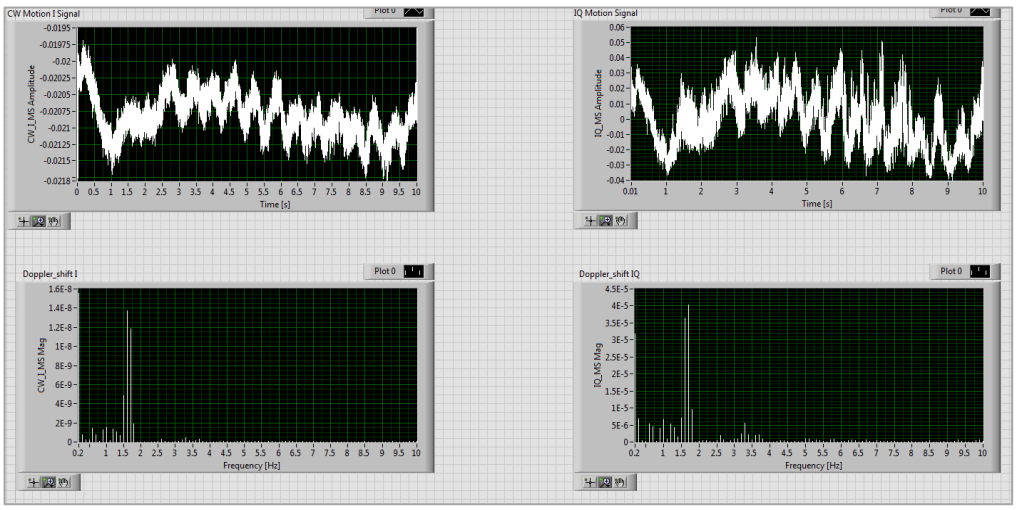

Figure 42 - Detected vibrations

2.2. LabView software modules

Inside the application are included different modules intended to reproduce, by software, the RF operations typically made in hardware. The main modules, implemented in LabView, are given below.

- **Signals generation.**

The signals generation software module is intended for 16 bit samples generation of the I and Q components to be transferred to the modulator. In order to produce a monochrome signal, it is necessary that the IQ components are cosinusoidal signals with a phase shift among them of 90°. The Figure 43 shown the LabView module implemented.

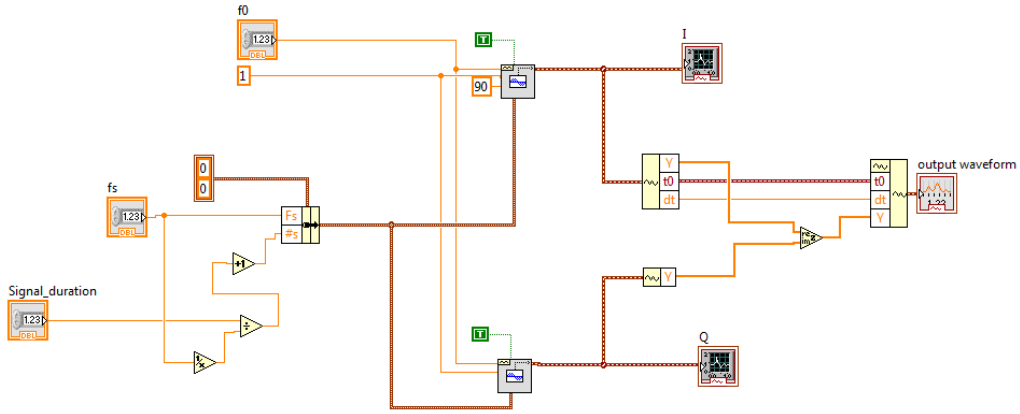

Figure 43 - Signals generation LabView module

A samples copy generated for the transmission is transferred to the following modules for the beat operation implementation.

- **IQ components beating**

The beat modules are hardwired to output signals with sum and difference frequency of the input signals frequencies. In the specific case, it is necessary to clean up the received signal by the transmitted signal contribution for extracting the phase containing information on the interest object motion. The physical beating operation is analytically reproducible through the multiplication, sample by sample, of the transmitted and received signals I and Q components. Figure 44 represents the implemented LabView modules.

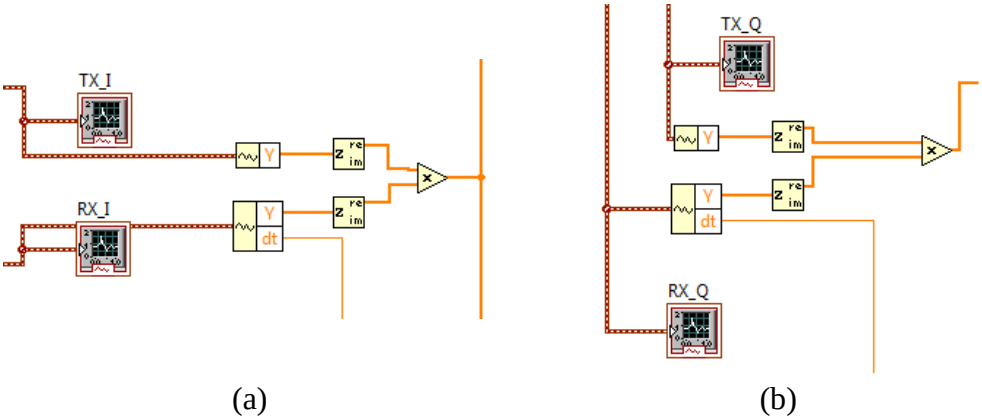

Figure 44 - Transmitted and received (a) I and (b) Q components beating

- **Extraction of the phase containing motion information**

Once that the IQ components have been pre-elaborate it is possible to extract the phase containing the oscillating motion information according to the diagram represented in Figure 19 described by the analytical expression referred in eq. (83). The LabView module related to these operations is represented in Figure 45.

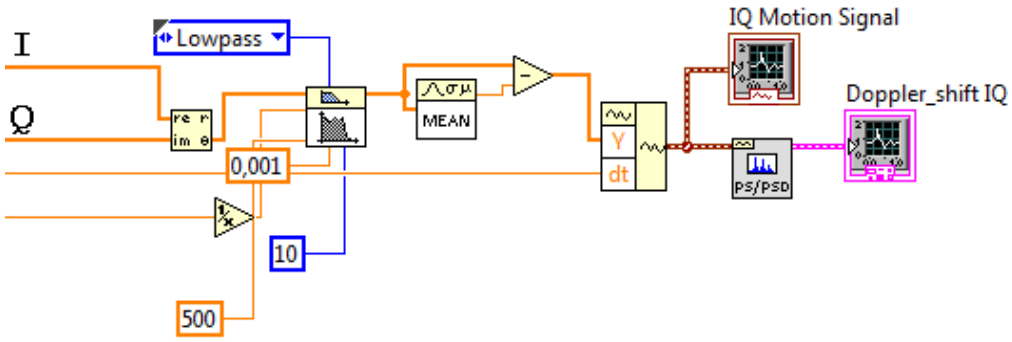

Figure 45 - Extraction of the phase containing targets motion information according to the IQ CW elaboration

The insertion of a lowpass filter following to the phase extraction module from the real and imaginary signal components allows to turn down the signal bandwidth to the opportune magnitude order to observe the interest vibrations, in order to decrease the samples number avoiding the aliasing phenomenon. The following module removes the signal mean value, coherently with those reported in eq. (84) (Figure 46).

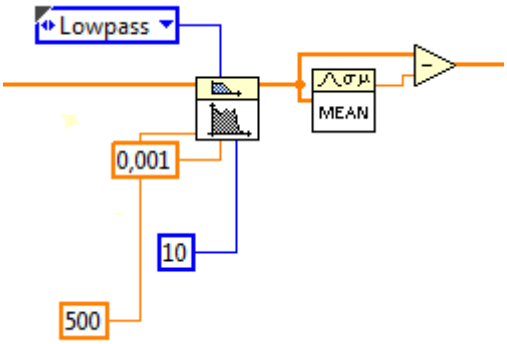

Figure 46 - Lowpass filter and the continuous component removal from the signal extracted

- **Lowpass filter**

In the elaboration flow of the signals, is required more times to filter the signal through a lowpass filter. This necessity exists in both the classical CW elaboration flow and the IQ CW elaboration as shown in Figure 38. The use of the filter is necessary for two different circumstances, such as the signals bandwidth reduction to reduce the samples number avoiding the aliasing phenomenon as stated above, but also to eliminate the "sum" frequency produced by the beat operation as shown in Figure 47.

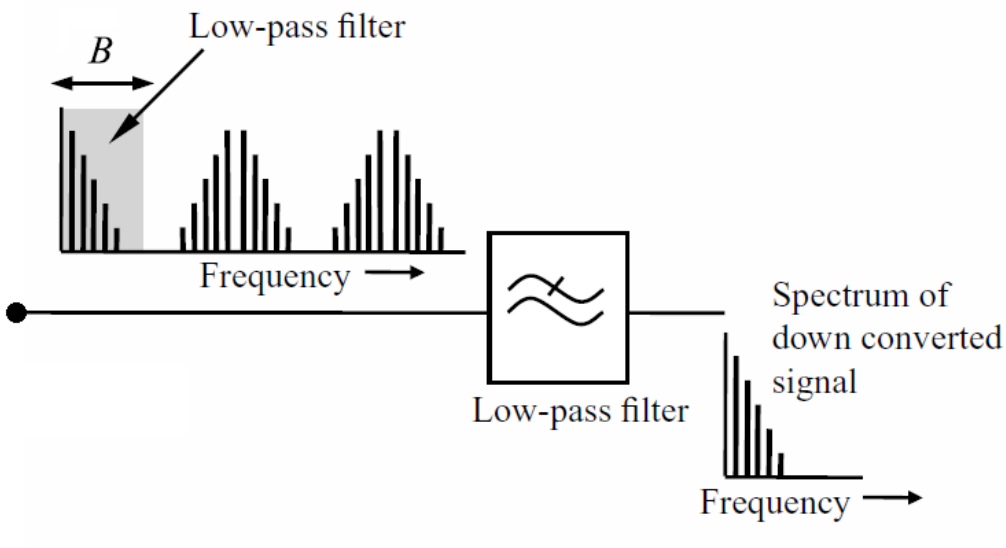

Figure 47 - Signal model and corresponding block schematic (courtesy of [55])

The used filter is a Chebyshev filter, whose typical frequency response has shown in Figure 48.

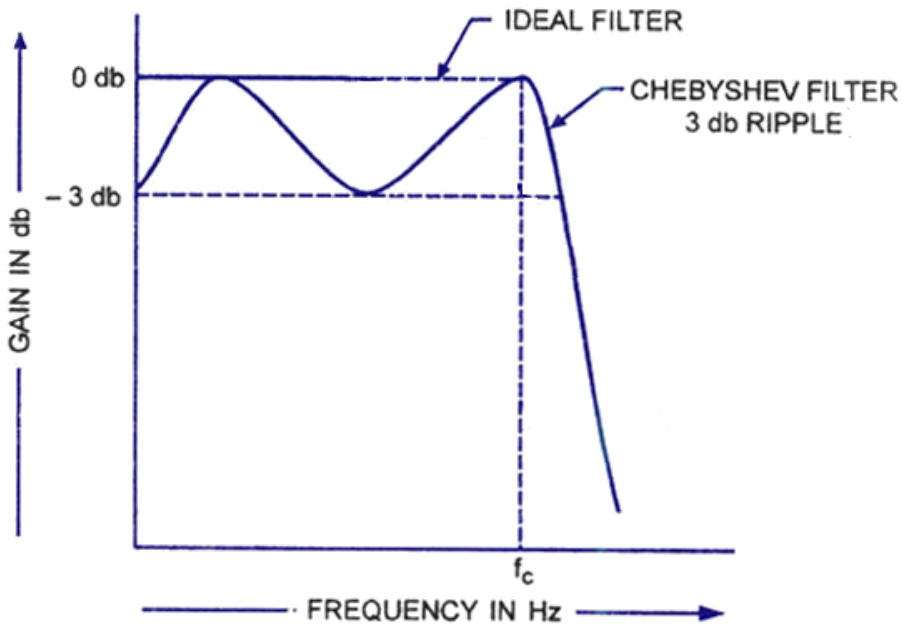

Figure 48 - Typical Chebyshev filter response

The filter used meets the request to have a very steep response that allows the filter to be more selective in frequency, counterbalanced by the disadvantage to having an elevated ripple bandwidth. As already shown in Figure 46, has been used a Chebyshev lowpass filter of tenth order, with a ripple bandwidth of 0.001 dB.

- **Samples decimation or Digital Down Conversion**

After the filtering with the lowpass filter is possible to decrease the sampling frequency, and therefore the samples number, through the opportune decimation of the samples vectors. This operation relieves the software elaboration and decreases the data dimension to be stored without resolution and detail losses. The LabView module related to these operations is represented in Figure 49.

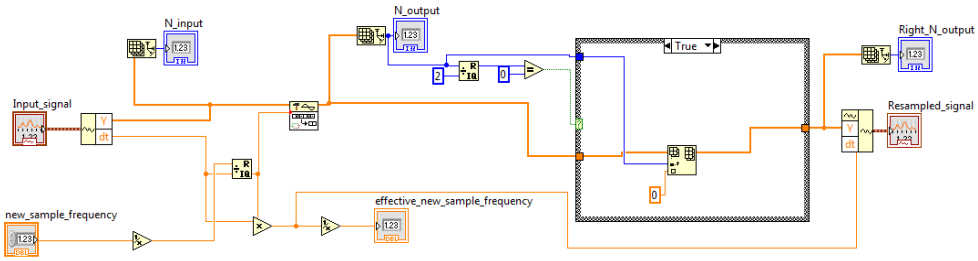

Figure 49 - Digital Down Conversion

- **Fast Fourier Transform and results visualization**

The reconstructions results are video displayed, in the time domain and in the frequency domain using the modules represented in Figure 50.

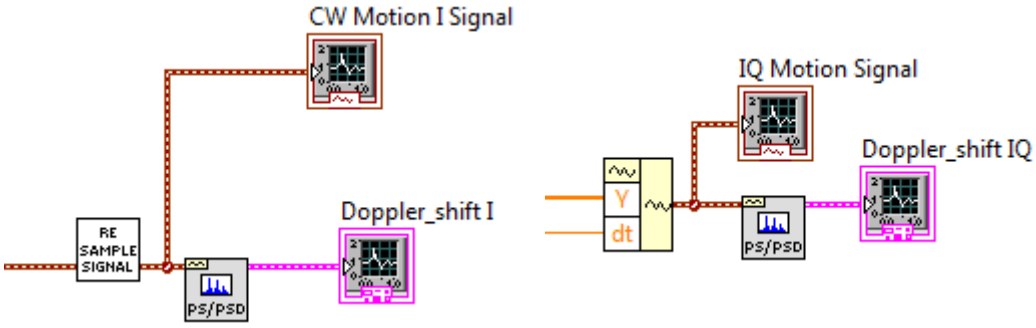

(a) (b)

Figure 50 - FFT and results plot (a) classic CW and (b) IQ CW

3. Experimental results with classical CW approach

In order to test the SDRadar functionality, experimental validations are performed [56-57].

As a first test, the displacement produced by the vibrating membrane of a standard speaker is considered. By connecting the speaker to the output of a PC sound card, through audio signal generation software, it is possible to produce a variable frequency membrane displacement. For a standard speaker, the membrane displacement $x(t)$ is on the order of 0.1 mm. With reference to the schemes in Figure 9 and Figure 10, the antennas and the target are placed at a mutual distance d_0 equal to 5 cm (Figure 51). The experimental setup diagram is shown in Figure 52.

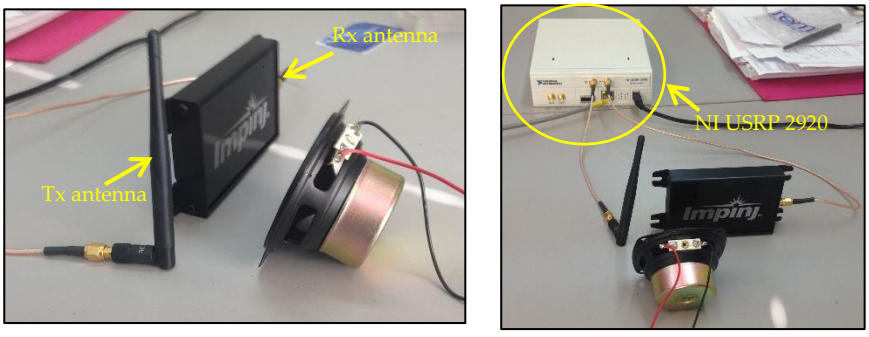

(a) (b)

Figure 51 - Experimental setup: (a) vibrating membrane in the presence of Tx and Rx antennas; (b) full SDRadar Doppler configuration.

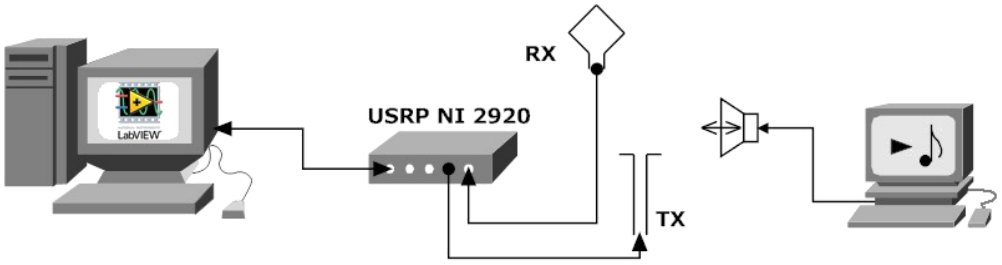

Figure 52 - Experimental setup diagram

For the validation test, we set $f_{IF} = 20\ kHz$ and $f_c = 1\ GHz$. Displacement data $x(t)$ related to a captured scene (at a given time) are illustrated in the time domain (Figure 53(a)) as well as in the frequency domain (Figure 53(b)). In particular, in the second figure, it is easy to distinguish the maximum peak giving the oscillation frequency f_m of the membrane, equal to $200\ Hz$ in the examined case.

The SDRadar Doppler platform is validated through various experimental tests, by producing vibrations with different oscillation frequencies. The related experimental results are summarized in Table 6 and compared in Figure 54. In particular, a relative error equal to zero is obtained in the reconstructed oscillation frequency, for all tests.

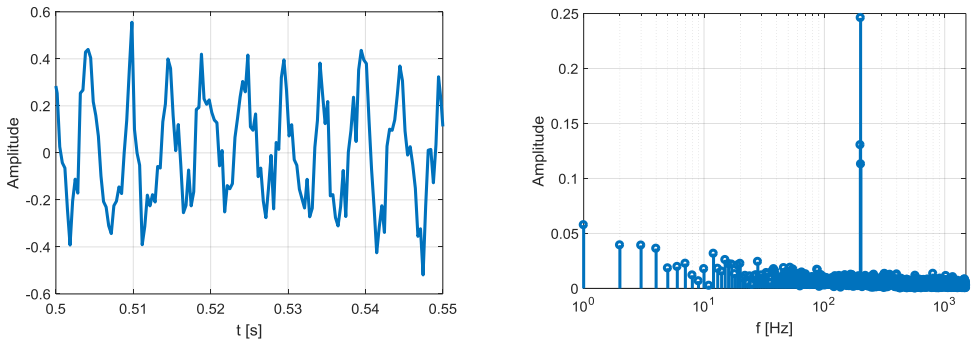

(a) (b)

Figure 53 - Captured scene in the presence of an oscillating target: (a) time domain; (b) frequency domain

Table 6 - Parameters and results of the first experimental validation test

B	f_{max}	T_0	Δf	f_m	f_m **(Identified)**
3 kHz	1.5 kHz	1 s	1 Hz	20 Hz	20 Hz
3 kHz	1.5 kHz	1 s	1 Hz	100 Hz	100 Hz
3 kHz	1.5 kHz	1 s	1 Hz	200 Hz	200 Hz
3 kHz	1.5 kHz	1 s	1 Hz	300 Hz	300 Hz

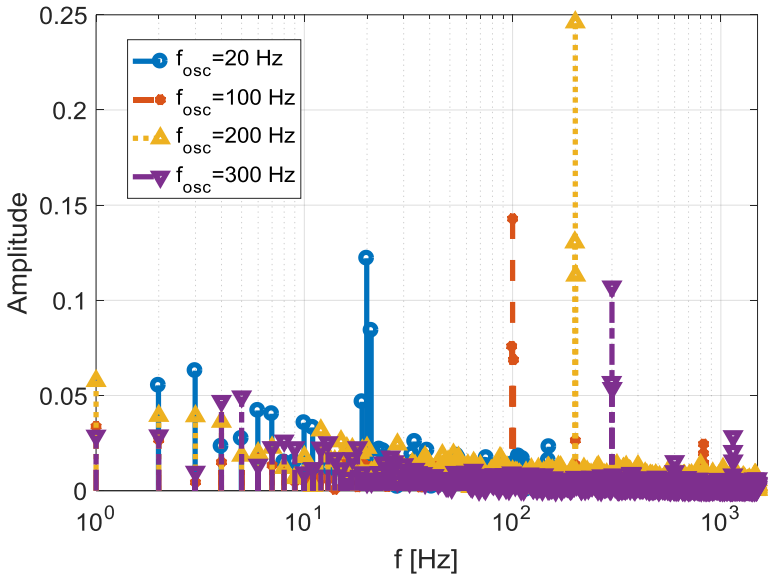

Figure 54 - Results of the first experimental validation test

In order to verify the SDRadar ability in distinguishing targets with oscillation frequencies shifted by a single resolution step, the same experiment is performed with different acquisition intervals. The results are shown in Table 7 and reported in Figure 55. In particular, when properly increasing the acquisition time T_0, a decrease of the relative error (from 0.16% down to 0.04%) is successfully observed.

Table 7 - Parameters and results of the second experimental validation test

B	f_{max}	T_0	Δf	f_m	f_m **(Identified)**
300 Hz	150 Hz	2 s	1/2 Hz	50 Hz	49.92 Hz
300 Hz	150 Hz	2 s	1/2 Hz	50.5 Hz	50.42 Hz
300 Hz	150 Hz	3 s	1/3 Hz	50.3 Hz	50.28 Hz

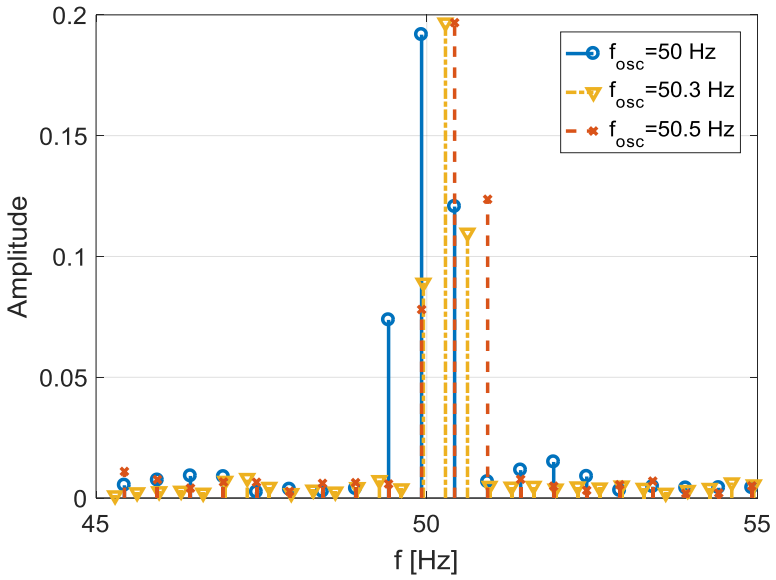

Figure 55 - Results of the second experimental validation test

The audio speaker as the one adopted in the first experimental test is able to produce vibrations limited to a minimum frequency of around 20 Hz. Thus, in order to verify the capabilities of the proposed SDRadar system at very low frequencies, a second experimental setup is considered. It is realized by applying a small metal target on the axis of a stepper micro motor controlled through an Arduino UNO (Arduino LLC, Ivrea, Italy) (Figure 56). The antennas and the target are placed at the same distances as in the previous test (Figure 57).

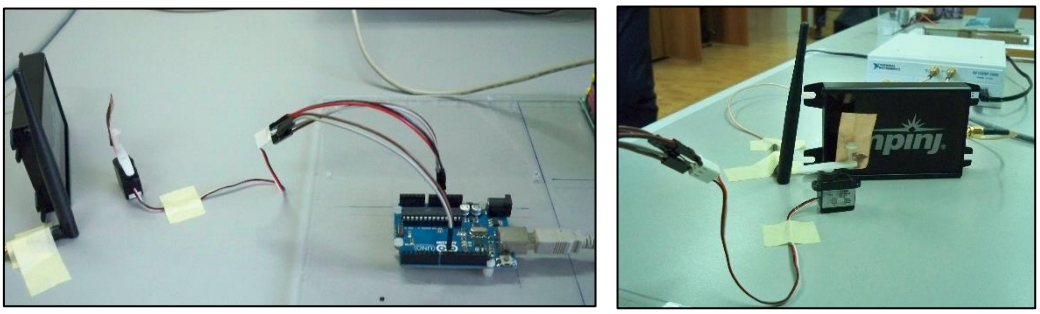

(a) (b)

Figure 56 - Setup of the second experimental test: (a) stepper micro motor connected to Arduino UNO (Arduino LLC, Ivrea, Italy); (b) stepper micro motor with a target in the presence of Tx and Rx antennas

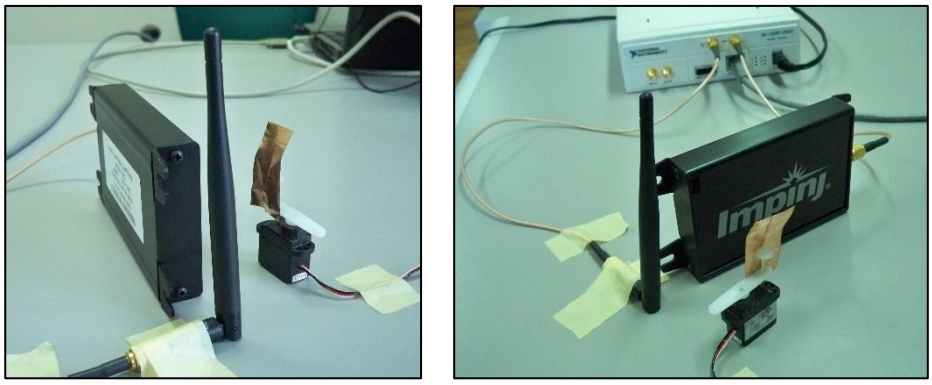

(a) (b)

Figure 57 - . Setup of the second experimental test: (a) stepper micro motor with target in the presence of Tx and Rx antennas; (b) full SDRadar Doppler configuration on the second scenario

A summary of all experimental results relative to the experimental setup of Figure 56 and Figure 57 is reported in Table 8, while the relative amplitude spectra are shown in Figure 58. The achieved results properly highlight the system capability to detect oscillations at frequencies below 10 Hz. In particular, a relative error equal to zero can be observed in the reconstruction of the oscillation frequency.

Table 8 - Parameters and results of the experimental validation tests on the second scenario

B	f_{max}	T_0	Δf	f_m	f_m **(Identified)**
3 kHz	1.5 kHz	100 s	0.01 Hz	0.3 Hz	0.3 Hz
3 kHz	1.5 kHz	100 s	0.01 Hz	1 Hz	1 Hz
3 kHz	1.5 kHz	100 s	0.01 Hz	5 Hz	5 Hz

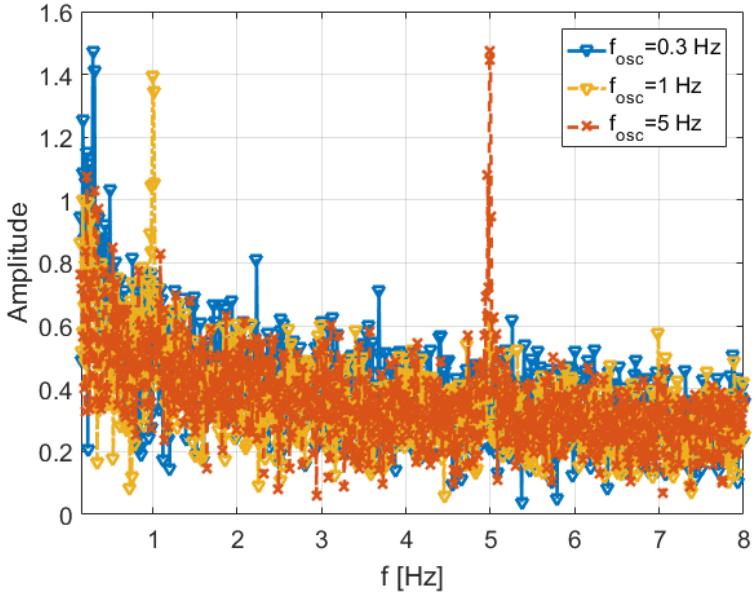

Figure 58 - Results of the experimental validation tests on the second scenario

As a further test, the generated audio signal performing a frequency sweep is considered. By monitoring the maximum peak frequency within a time window equal to 35 s (Figure 59), an increase over time of the detected oscillation frequency f_m is obtained.

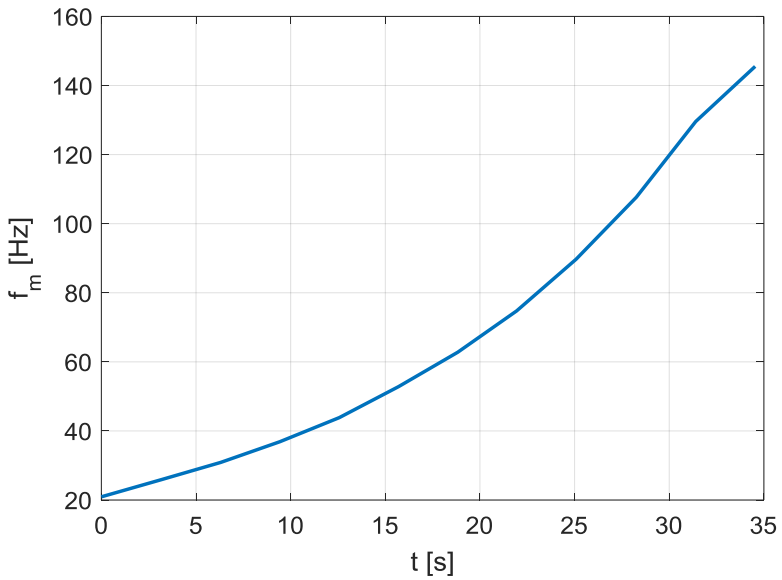

Figure 59 - Monitoring of the target oscillation frequency within a time window of 35 s

4. Experimental results with IQ CW approach: breath detection

As noted above, the SDRadar platform has been developed for targets motion reconstruction through the classical CW elaboration or with the IQ CW elaboration only using further LabView software modules.

The experimental tests carried out through the classical CW approach, described in the previous paragraph, showed a good ability of the platform to properly detect the vibrations frequency in a wideband, with elevated resolution and varying, in a dynamic way, the radar parameters. Nevertheless, the vibrations amplitude detection uncertainty and the distortion effects of this value caused by the "Null Detection Points" presence, analyzed in the previous chapter, did not allow to effect an estimate of the movement amplitude entity.

The showed tests following intended to take two goals:

- to effect a complete target motion reconstruction both in terms of frequency and in terms of amplitude;

- to identify, through the developed platform, different respiratory abilities conditions of a human subject.

For that purpose, the previous setup has been rearranged making a rigid support for the antennas (Figure 60) to place in monitored subject proximity.

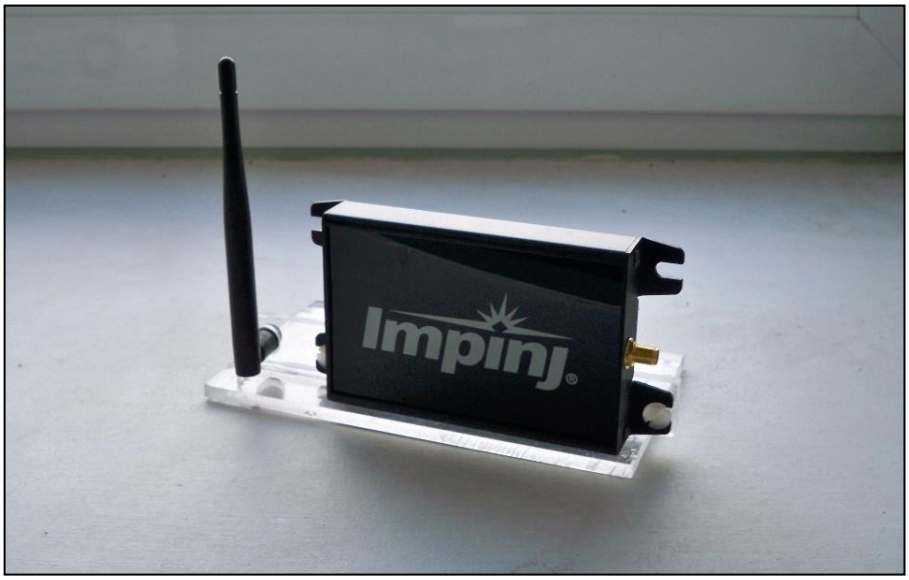

Figure 60 - Antennas installed on their support

The antenna system has been therefore turned in such way that the receiving antenna aimed at the subject abdomen, as shown in Figure 61.

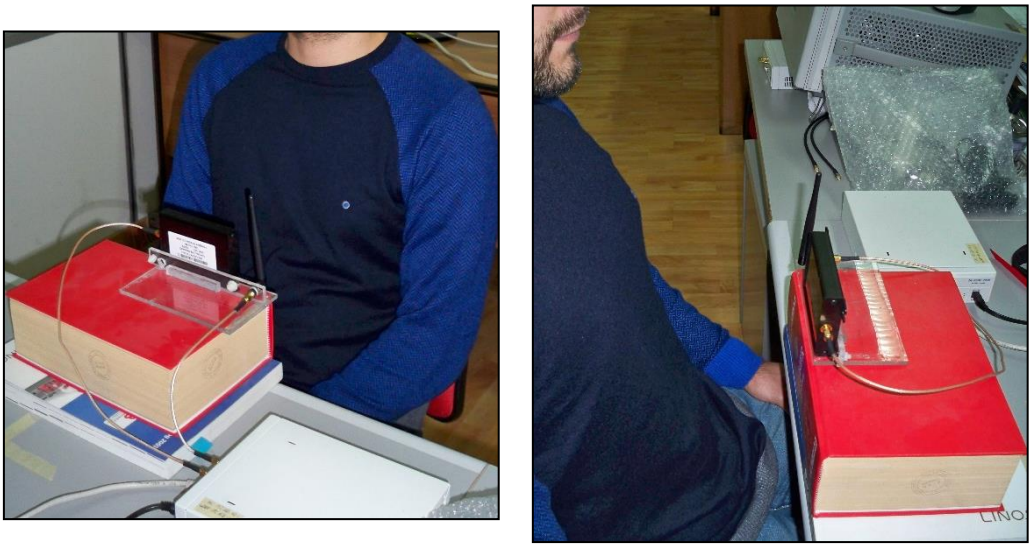

(a) (b)

Figure 61 - . Subject position in relation to the antennas: (a) frontal view; (b) side view

For these tests we set, by the SDRadar system software interface fc=820MHz and fIF=20 KHz, to work to one of the frequencies previously identified. An acquisition interval T0=10 s has been fixed.

The subject under observation has faked three different conditions:

- normal respiration;
- accelerated respiration;
- interrupted respiration.

The acquired data have shown the system ability to detect the abdominal movements due to the respiratory activity but the presence of irregularity in the in collected data (Figure 62) requested further post elaborations execution.

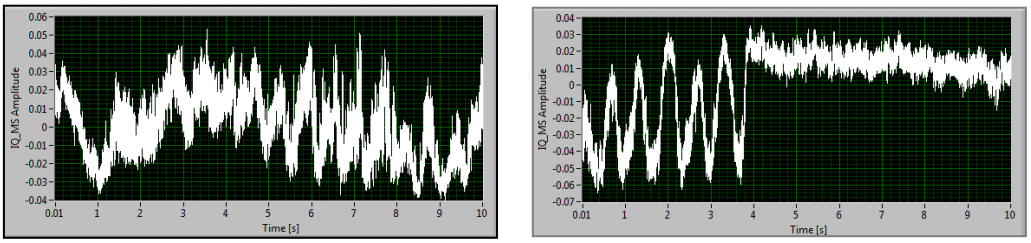

(a) (b)

Figure 62 - Detected movements visualized in the system video interface: (a) accelerated respiration; (b) interrupted respiration

To reduce the irregularities, and to smooth therefore the signals, a filtering has been effected in Matlab environment through a mobile average window.

a. Normal respiration

In the first reported case, the subject, without making some further movements, has breathed in a regular way during the observation interval.

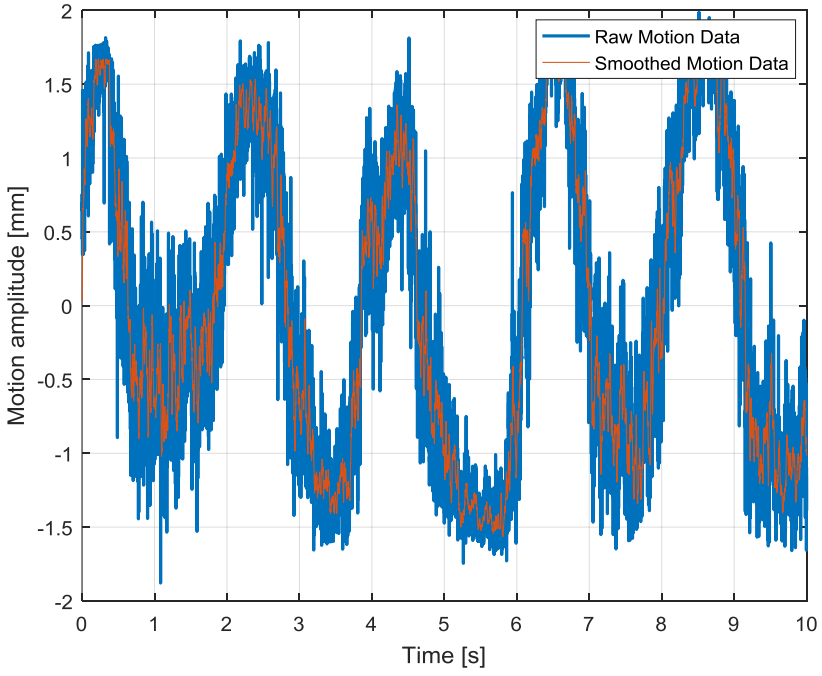

Figure 63 - Detected movement during the normal respiratory activity

The detected movement (Figure 63), in particular after the smoothing, looks very regular and underlines an abdominal shift during the normal respiratory activity of around 3 mm (from around 1.7 mm during the maximum expansion to around -1.5 mm at the expiration end).

Through the spectral analysis it is possible to estimate the subject breath rate as shown in Figure 64.

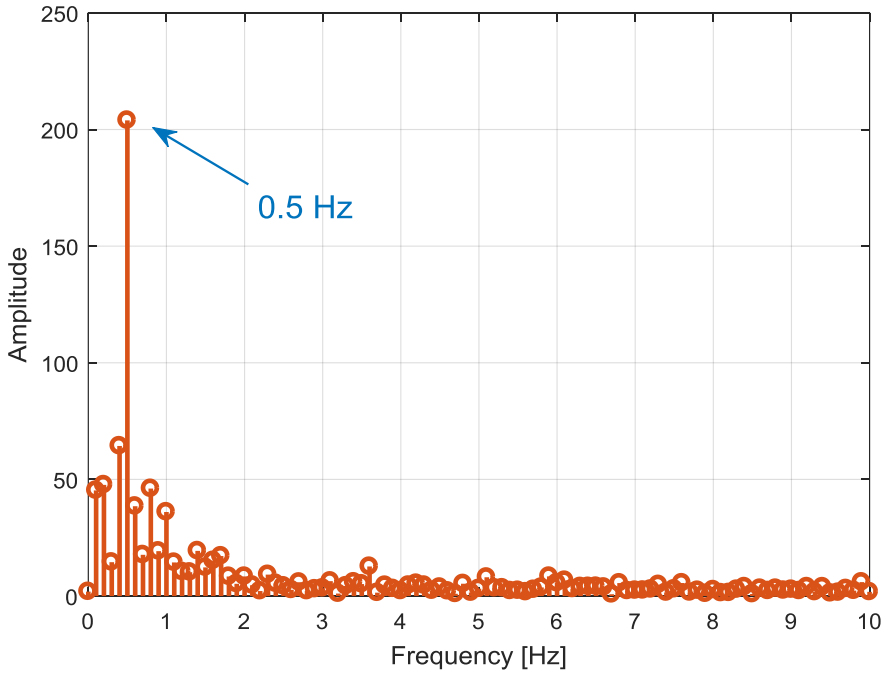

Figure 64 - Detected normal respiration movement spectrum

The breath rate detected corresponds to the frequency of 0.5 Hz. The parameters and results related to this experiment are summarized in Table 9.

Table 9 - Parameters and results of the experimental test related to the normal respiration

B	1 kHz
f_{max}	500 Hz
T_0	10 s
Δf	0.1 Hz
f_m **(Identified)**	0.5 Hz
Breath rate	30 breaths/min

b. Accelerated respiration

In the second considered case, the subject switched by a normal respiratory activity to a respiratory activity forcibly accelerated.

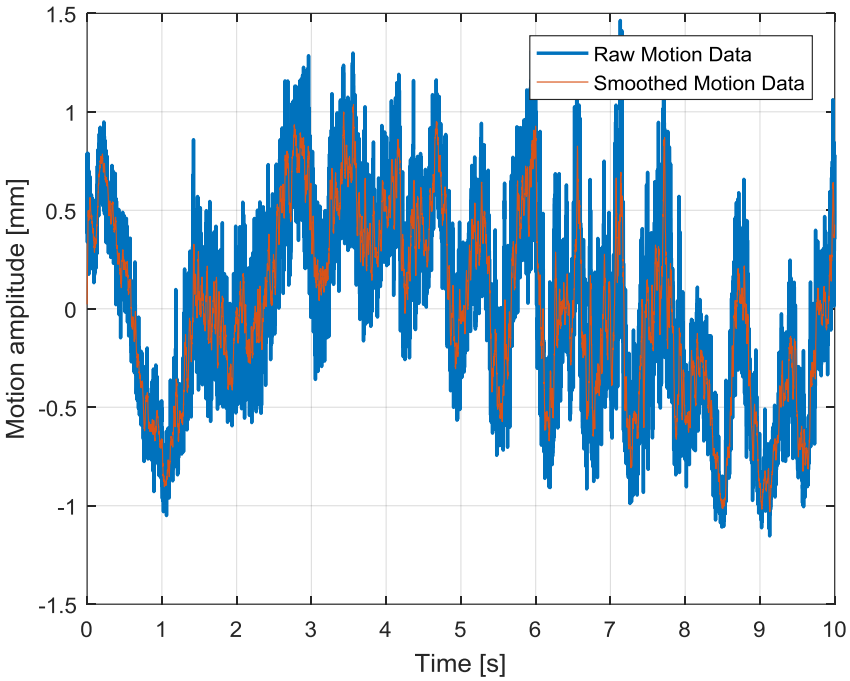

Figure 65 - Detected movement during the accelerated respiratory activity

The respiratory movement shows a great frequency and a smaller excursion, characteristics typical of an accelerated respiratory activity. Probably the measure is partially influenced by a slight body movement, appreciable observing the detected movement trend (Figure 65).

Also in this case, through the spectral analysis it is possible to estimate the subject breath rate as shown in Figure 66.

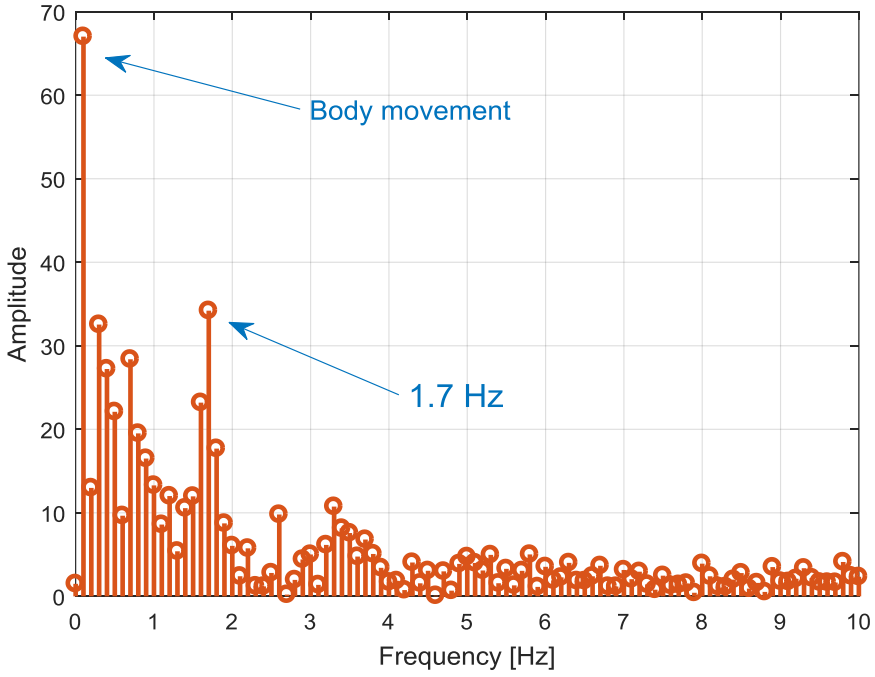

Figure 66 - Detected accelerated respiration movement spectrum

Table 10 - Parameters and results of the experimental test related to the accelerated respiration

B	1 kHz
fmax	500 Hz
T_0	10 s
Δf	0.1 Hz
***fm* (Identified)**	1.7 Hz
Breath rate	102 breaths/min

c. Interrupted respiration

In the last considered case, the subject interrupts the respiratory activity, switching so by an accelerated respiratory activity to the complete activity absence.

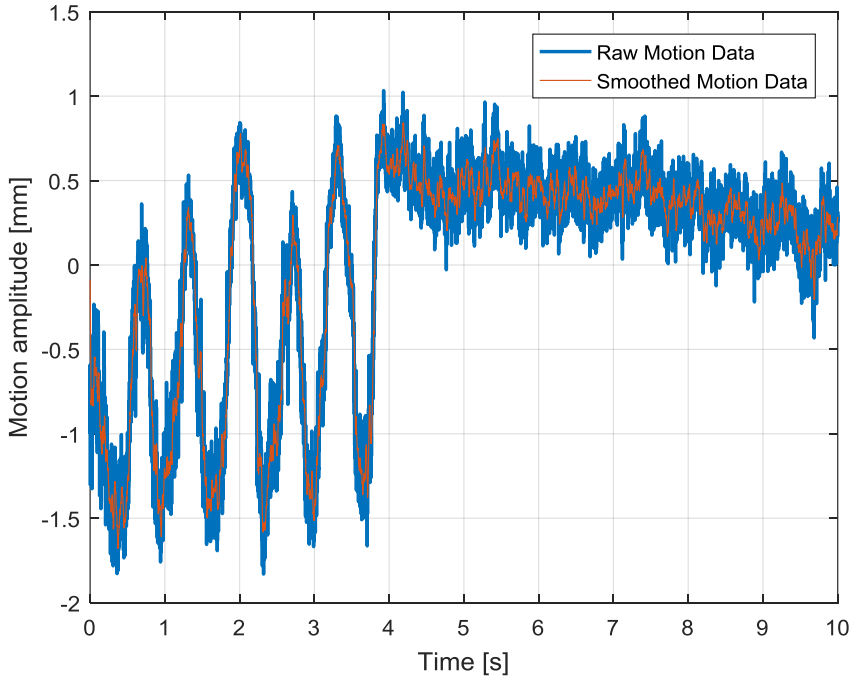

Figure 67 - Detected movement during the interruption of the respiratory activity

In this case, it is immediately distinguishable the difference between the two types of respiratory activity and therefore it is possible to discriminate these conditions in an easy way.

5. System performances

Finally, as a quantitative analysis of the performances relative to the proposed SDRadar Doppler approach, the response time is evaluated for different values of the acquisition time T_0. Data reported in Table 11, indicating the average value of

the radar elaboration time and response time, are obtained from a set of 50 acquisitions for each value of assumed time T_0.

Table 11 - Radar elaboration time and system response time

T_0 (s)	Radar Elaboration Time (s)	System Response Time (s)
10^{-3}	2.040	2.041
10^{-2}	2.120	2.130
6×10^{-1}	2.083	2.683
1	2.124	3.124
2	2.223	4.223
3	3.320	6.320

Conclusions

In this job, a SDRadar Doppler platform has been proposed and implemented for the vibrations detection and more in the specific for physiological movements as such.

In the first part of the elaborate, after introducing the job motivations, a careful study of the reference literature has been carried out. From this investigation, the actual invasive and in contact monitoring methods limits have emerged and the cases to which the physiological parameters noninvasive monitoring would bring notable benefits have been identified. The stock of the situation on the technologies already experimented and currently available has been made. Following, a brief mention on the radars, analyzing their technical and scientific evolution, their operation and the different typologies of them has been made. From the analysis, opportunities for the monitoring and the individualization of target offered in radar framework from the effect Doppler have emerged The last part reserved to the state of the art has been devoted to the Software-Defined Radio devices and to the potentialities offered by this technology, choice as hardware support for the proposed job.

In the second part of the elaborate, has been described, theoretically and analytically, the CW Doppler radars operation and the methods to use these devices for the targets motion detection. Particularly, besides furnishing a detailed analytical model that describes the radar operation, the advantages and the disadvantages of this solution and the possibility to overcome the limits introduced through the signals IQ modulation have been individualized.

In the third part of the elaborate, the implemented platform has been described, from the hardware point of view and from the software point of view. Particularly an SDRadar platform that traces the functional statements models stated above has been implemented. Through a series of experimental tests, the platform abilities to detect artificial vibrating motions have been tested and in last the experimental tests on human subjects with the purpose to detect different respiratory activity conditions have been realized. The tests have shown the implemented system ability to properly detect, both in terms of frequency and in terms of ampleness, the vibrating motions and the respiratory activity.

The work done reserve opportunity for further developments. Particularly, opportunity to equip the SDRadar platform with the modern antennas systems that implement beamforming techniques would endow the platform, and in a particolar way the radiant part, of great flexibility and efficiency and therefore of best physiological phenomena sensing abilities.

Appendix – Reconfigurable Reflectarray antenna with high beam scanning

During the Ph.D. I followed another distinct research lines, also located in the scientific field of electromagnetics.

1. Problem description

The applications based on the modern RF systems require increasingly the possibility to have flexible radiant elements, such to be able to dynamically support different coverage demands. Significant examples may also be found in radar applications for remote sensing or to military use, in which it is necessary to quickly scan large angular regions or in mobile applications, where may be necessary to direct the antenna in dynamically in the maximum radiation direction with the purpose to maximize the gain.

2. State of the art

Different types of approach exist for the antennas implementation with characteristics that allow realizing the beam scanning:

- Mechanic Approach - Reflector antennas with motorized movable feed
- Electronic Approach - Antennas who base their operation on the use of electrical components with controllable characteristics, as for example lengths of the load line or metallization controlled through the selective pilotage of RF switch or antennas array in which at every single element is related a varying reactive load.

Following, the principal characteristics of the technologies listed above are provided.

Technology		Characteristics
Reconfigurable antennas through mechanic approach		The presence of motors implicates the necessity to have driving and control circuits and considerable energy expenditure. It's about of bulky structures, subject to vibrations and mechanical solicitations that reduce the reliability and the lifetime, and negatively influence the scanning speed.
Reconfigurable antennas through electronic approach	Phased array	It is a matrix of antennas where every element or group of elements is fed through an electronically controlled phase-shifter and amplifiers. As the number of elements increases it notably also increases the hardware complexity, with the consequent complication of the control net, that also engraves negatively in the cost and in the encumbrance of the structure. Besides, the elevated components number in the feeding net introduces elevated losses.
	Reflectarray with varying reactive load	The currently solutions present in literature involve the association than at least two varactor diodes for every reflectarray element. Complex and expensive control net.

The objective of this research line consists in the development of a Reflectarray composed of an aperture coupled rectangular patch antennas array. On every element of the array is present a varying reactive load constituted by only one varactor diode, with the purpose to realize a complete phase control of the reflected field. This solution unlike others present in literature that use at least two varactor diodes, allow notable simplifications of the feeding lines, with consequent simplification also in the control electronics.

3. Results

The first phase of the Reflectarray development consists in the single element design that will go to constitute the array, which will presumably be composed by around one hundred elements. The single element has been developed and experimentally validated by a measurement campaign implemented in the UNICAL Microwaves Laboratory. In Figure 68 are shown the elementary cell layout, whose dimensions are summarized in Table 12.

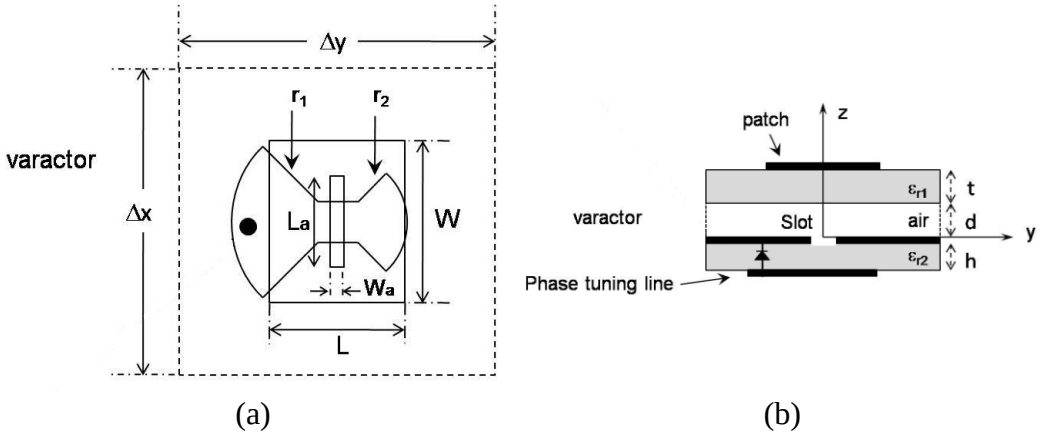

(a) (b)

Figure 68 - Elementary cell layout: (a) top view; (b) side view

Table 12 - Dimensions and physical characteristics of the elementary cell

L	8.9 mm	**t**	0.762 mm
La	6.7 mm	**d**	1.524 mm
W	6.8 mm	**h**	0.762 mm
Wa	0.7 mm	**ε_{r1}**	2.33
r1	4.3 mm	**ε_{r2}**	6.15
r2	2.7 mm		

A varactor diode has been chosen as varying reactive load with a junction capacity that varies from 0.2pF to 20pF. The simulations carried out on the structure indicate that the designed cell allows a phase control, through the varactor diode capacity variation, of around 320° in the frequency range of [9.6. 10.45] GHz (Figure 69).

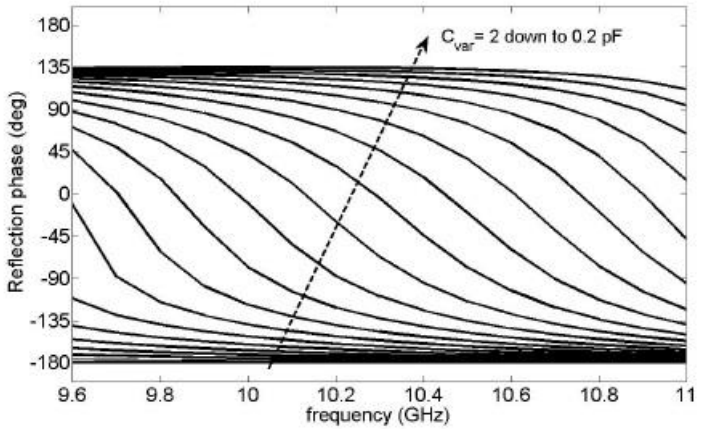

Figure 69 - Simulation of the reflection phase vs. frequency with different junction capacity

In order to experimentally validate the structure, a square array prototype composed by 25 elements has been realized. The radiant structure has been accompanied by an electronic card able to produce in dynamically the polarization voltages for the varactor diodes. Finally, a measurement setup has been prepared

inside the Microwaves Laboratory anechoic chamber (Figure 70) to perform the necessary measures to the experimental validation.

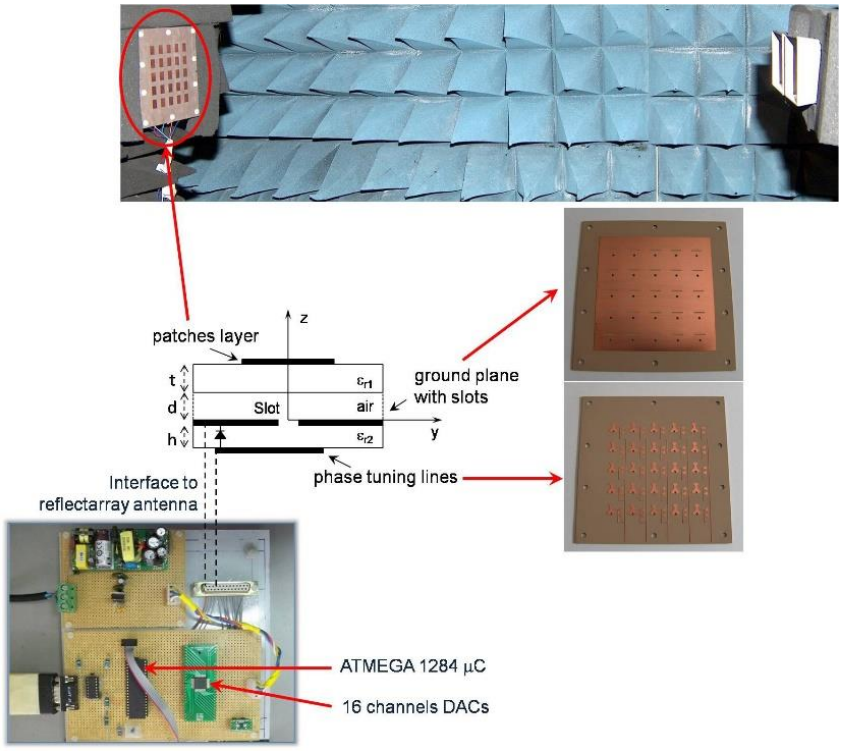

Figure 70 - Measurement setup

The measures carried out result conforming to the simulations results, as shown in Figure 71.

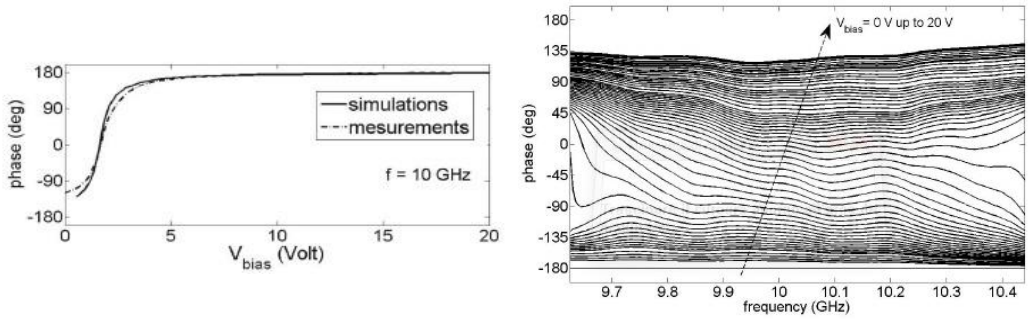

(a) (b)

Figure 71 - (a) Phase measure vs. center band simulation (10 GHz); (b) Simulation of the reflection phase vs. frequency with different polarization voltages

4. Personal contribution to the research

The main personal activity inside the research line previously exposed has concerned the development of the electronic card devoted to the dynamic

generation of the varactor diodes polarization voltage. Particularly, an electronic card prototype has been realized whose core is constituted by a microcontroller responsible to receive from a PC through the RS-232 serial interface the voltages vector to be applied to the varactor diodes. The microcontroller, on which a micro-programme specially designed is performed, will take care therefore to transfer, through the digital interface, the opportune commands to every DACs, in such way that they can produce the demanded voltages.

(μC) Atmel ATMEGA1284P has been chosen as a microcontroller. This μC is equipped with 128KB of memory Flash, an EEPROM of 4KB and an internal SRAM of 16KB. The microcontroller has, besides, USART and SPI digital serial interfaces, which can be used for establishing a communication between the μC and a PC (USART) and between the μC and the DACs (SPI).

The Reflectarray performances are strongly dependent on the accuracy with which the varactor diodes is polarized. The specifications taken into account in the DAC choice are the voltage range to apply to the single varactor (0V. 20V) and the least required variation among the voltage levels (0.01V). These characteristics have induced to select the integrated circuit (IC) AD5360 produced by Analog Device, whose characteristics are illustrated in Table 13.

Table 13 - AD5360 characteristic

	AD5360	
Channels	*16*	
Power supply	*Dual*	
V_{DD}	*-0.3V to +17V*	
V_{SS}	*-17V to +0.3V*	
Reference voltage	*External*	
V_{FSR}	*20V*	
Output voltage range	*Reference*	
	2.5V	*-5V to +5V*
	5V	*-10V to +10V*
Resolution	*16 bits*	
LSB	$3.05 * 10^{-4}$	
Relative error	*+/-4 LSB max*	
Digital interface	*SPI*	

The 16 available channels on a single integrated circuit allow to reduce the components number and the connections complexity on the prototype. The SPI interface is perfectly compatible with the μC.

To get the output voltages range, in order to realize an excursion of 20V, has been chosen to use as 5V external reference the integrated circuit AD435 of Analog Device.

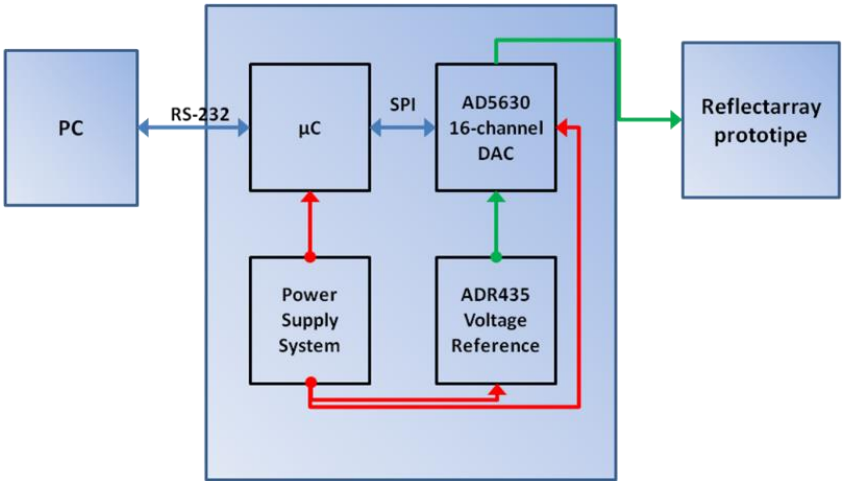

Figure 72 - Electronic card block diagram

The introduced architecture (Figure 72) allows increasing in a simple way the number of output DAC channels (Figure 73). In fact, the SPI bus, with µC as master of the communication, can reach, in a parallel way, different AD5360 fixed as a slave device. Every IC has an enabling communication signal, therefore the µC selects case by case, in a sequential way, the IC with which it wants to communicate.

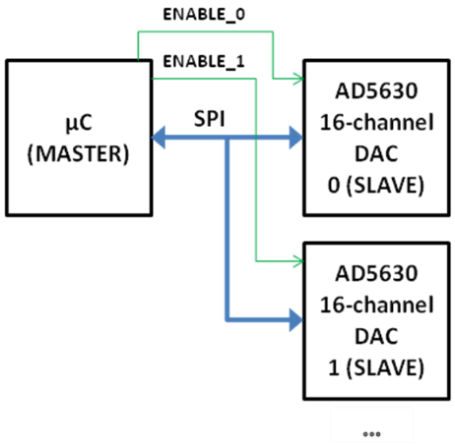

Figure 73 - Electronic card extension

The prototype has been realized with discrete components on a stripboard (Figure 74) and it has a 6 pins ISP interface to transfer the micro-programme on the µC.

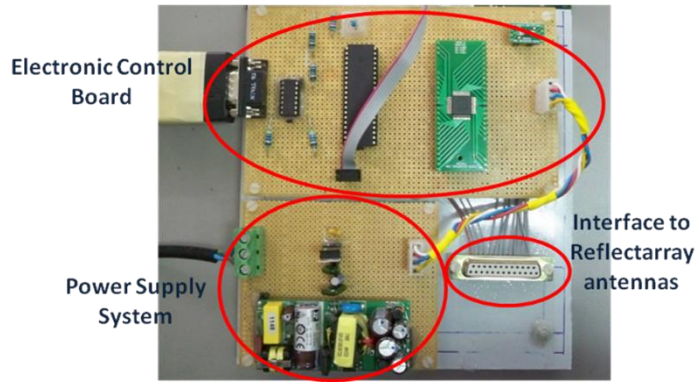

(a)

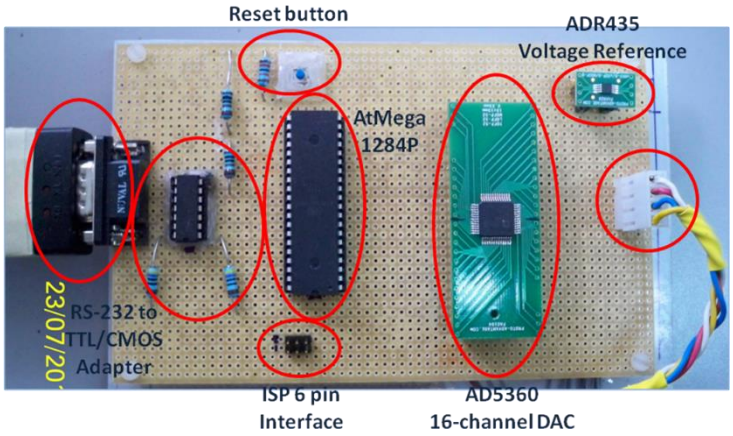

(b)

Figure 74 - (a) Electronic control card and power supply card; (b) control card

Finally, has been developed, in Matlab language, the communication software running on the PC to set the voltages to apply to the varactor diodes (Figure 75). Both the micro-programme running on the μC and the management software has been developed in such way as to be able to manage the electronic card equipped with maximum ten AD5360s.

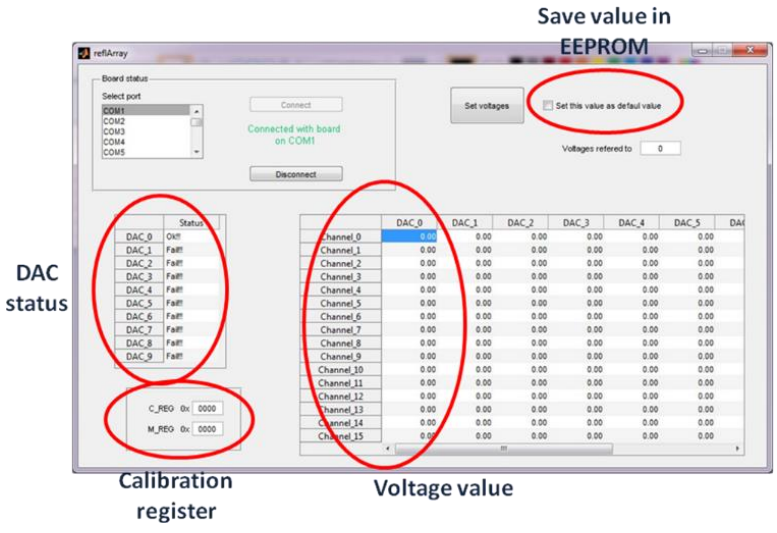

Figure 75 - Main communication software window

Bibliography

[1] I. Jung and Y. Roh, "Design and fabrication of piezoceramic bimorph vibration sensors," *Sens. Actuators A Phys.,* 1998.

[2] H. Sumali, K. Meissner and H. Cudney, "A piezoelectric array for sensing vibration modal coordinates," *Sens. Actuators A Phys.,* 2001.

[3] A. Vogl, D. Wang, P. Storås, T. Bakke, M. Taklo, A. Thomson and L. Balgård, "Design, process and characterisation of a high-performance vibration sensor for wireless condition monitoring," *Sens. Actuators A Phys.,* 2009.

[4] E. Peiner, D. Scholz, A. Schlachetzki and P. Hauptmann, "A micromachined vibration sensor based on control of power transmitted between optical fibres," *Sens. Actuators A Phys.,* 1998.

[5] G. Conforti, M. Brenci, A. Mencaglia and A. Mignani, "Fiber optic vibration sensor for remote monitoring in high power electric machines," *Appl. Opt.,* 1989.

[6] J. Zook, W. Herb, C. Basset, T. Stark, J. Schoess and M. Wilson, "Fiber-optic vibration sensor based on frequency modulation of light-excited oscillators.," *Sens. Actuators A Phys.,* 2000.

[7] M. Kimura and K. Toshima, "Vibration sensor using optical-fiber cantilever with bulb-lens.," *Sens. Actuators A Phys,* 1998.

[8] M. Jelic, D. Stupar, B. Dakic, J. Bajic, M. Slankamenac and M. Zivanov, "An intensiometric contactless vibration sensor with bundle optical fiber for real time vibration monitoring," *Proceedings of the 2012 IEEE 10th Jubilee International Symposium on Intelligent Systems and Informatics, Subotica, Serbia, 20–22 September 2012,* 2012.

[9] W. Palmetshofer, "Contactless vibration measurement for condition monitoring," *Asset Manag. Maint. J.,* 2016.

[10] M. Pieraccini, M. Fratini, F. Parrini, G. Macaluso and C. Atzeni, "High-speed CW step-frequency coherent radar for dynamic monitoring of civil engineering structures," *Electronics Letters,* 2004.

[11] G. Grazzini, M. Pieraccini, D. Dei and C. Atzeni, "Simple microwave sensor for remote detection of structural vibration," *Electronics Letters,* 2009.

[12] B. Lohman, O. Boric-Lubecke, V. Lubecke, P. Ong and M. Sondhi, "A digital signal processor for Doppler radar sensing of vital signs," *IEEE Engineering in Medicine and Biology Magazine,* 2002.

[13] C. Gu and C. Li, "Assessment of Human Respiration Patterns via Noncontact Sensing Using Doppler Multi-Radar System," *Sensors,* 2015.

[14] S. Costanzo, F. Spadafora, G. Di Massa, A. Borgia, A. Costanzo, G. Aloi, P. Pace, V. Loscri and H. Moreno, "Potentialities of USRP-based software defined radar systems," *Prog. Electromagn. Res. B,* 2013.

[15] S. Costanzo, F. Spadafora, A. Borgia, H. Moreno, A. Costanzo and G. Di Massa, "High Resolution Software Defined Radar System for Target Detection," *J. Electr. Comput. Eng.,* 2013.

[16] S. Costanzo, F. Spadafora, H. Moreno, T. Scarcella and G. Di Massa, "Multiband Software Defined Radar for Soil Discontinuities Detection," *J. Electr. Comput. Eng.,* 2013.

[17] S. Costanzo, G. Di Massa, A. Costanzo, A. Borgia, A. Raffo, G. Viggiani and P. Versace, "Software-Defined Radar System for Landslides Monitoring," *Adv. Intell. Syst. Comput.,* 2016.

[18] S. Costanzo, G. Di Massa, A. Costanzo, L. Morrone, A. Raffo, F. Spadafora, A. Borgia, G. Formetta, G. Capparelli and P. Versace, "Low-Cost Radars Integrated into a Landslide Early Warning System," *Adv. Intell. Syst. Comput.,* 2015.

[19] C. Li, V. Lubecke, O. Boric-Lubecke and J. Lin, "A review on recent advances in Doppler radar sensors for noncontact healthcare monitoring," *IEEE Trans Microwave Theory Tech,* 2013.

[20] L. Tarassenko, A. Hann and D. Yound, "Integrated monitoring and analysis for early warning of patient deterioration," *Br J Anaesth,* 2006.

[21] J. Webster, "Medical Instrumentation," *Wiley,* 2010.

[22] P. Colditz, K. Dunster, G. Joy and I. Robertson, "Anetoderma of prematurity in association with electrocardiographic electrodes," *J Am Acad Dermatol,* 1999.

[23] S. Loo, T. Kuo, G. Waters, M. Muller and T. Brown, "A mobile electrode for ECG monitoring," *Burns,* 2004.

[24] M. Kryger, T. Roth and W. Dement, "Principles and Practice of Sleep Medicine. 3rd ed," *Philadelphia: W.B. Sunders Co.,* 2000.

[25] U. Kiechl-Kohlendorfer, D. Hof, U. Peglow, B. Traweger-Ravanelli and S. Kiechl, "Epidemiology of apparent life threatening events," *Am Acad Pediatr Grand Rounds,* 2005.

[26] J. Lin, "Non-invasive microwave measurement of respiration," *Proc IEEE,* 1975.

[27] S. Sharpe, J. Seals, A. MacDonald and S. Crowgey, "Non-contact vital signs monitor," *US patent# 4,958,638.,* 1990.

[28] E. Staderini, "UWB radars in medicine," *IEEE Aerospace Electron Syst Mag,* 2002.

[29] J. Lin, J. Kiernicki, M. Kiernicki and P. Wollschlaeger, "Microwave apexcardiography," *IEEE Trans Microwave Theory Tech,* 1979.

[30] J. Lin, E. Dawe and J. Majcherek, "A noninvasive microwave apnea detector," *Proceedings of the San Diego Biomedical Symposium,* 1977.

[31] K. Chan and J. Lin, "Microprocessor-based cardiopulmonary rate monitor," *Med Biol Eng Comput,* 1987.

[32] E. Greneker, "Radar sensing of heartbeat and respiration at a distance with applications of the technology," *Radar 97 Conference Proceedings,* 1997.

[33] K. Chen, Y. Huang, J. Zhang and A. Norman, "Microwave life-detection systems for searching human subjects under earthquake rubble or behind barrier," *IEEE Trans Biomed Eng,* 2000.

[34] H. Chuang, Y. Chen and K. Chen, "Microprocessor-controlled automatic clutter-cancellation circuits for microwave systems to sense physiological movements remotely through the rubble," *Proceedings of the Instrumentation and Measurement Technology Conference,* 1990.

[35] J. Seals, S. Crowgey and S. Sharpe, "Electromagnetic vital signs monitor," *Georgia Tech Research Institute Biomedical Division, Atlanta, GA, Final Report Project A-3529-060,* 1986.

[36] N. Hafner, I. Mostafanezhad, V. Lubecke, O. Boric-Lubecke and A. Host-Madsen, "Non-contact cardiopulmonary sensing with a baby monitor," *Engineering in Medicine and Biology Society, 2007. EMBS 2007. 29th Annual International Conference of the IEEE,* 2007.

[37] A. Singh, M. Baboli, X. Gao, E. Yavari, B. Padasdao, B. Soll, O. Boric-Lubecke and V. Lubecke, "Considerations for integration of a physiological radar monitoring system with gold standard clinical sleep monitoring systems," *35th Annual International Conference of the IEEE Engineering inMedicine and Biology Society (EMBC),* 2013.

[38] A. Droitcour, T. Seto, P. Byung-Kwon, S. Yamada, A. Vergara, C. El Hourani and T. Shing, "Non-contact respiratory rate measurement validation for hospitalized patients," *Engineering in Medicine and Biology Society, 2009, EMBC 2009. Annual International Conference of the IEEE,* 2009.

[39] A. Vergara, N. Petrochilos, O. Boric-Lubecke, A. Host-Madsen and V. Lubecke, "Blind source separation of human body motion using direct conversion Doppler radar," *IEEE MTT-S International Microwave Symposium Digest,* 2008.

[40] C. Gu, C. Li, J. Lin, J. Long, J. Huangfu and L. Ran, "Instrument-based noncontact Doppler radar vital sign detection system using heterodyne digital quadrature demodulation architecture," *IEEE Trans Instrum Meas,* 2010.

[41] A. Droitcour, O. Boric-Lubecke, V. Lubecke and J. Lin, "0.25 μm CMOS and BiCMOS single-chip direct-conversion Doppler radars for remote sensing of vital signs," *IEEE International Solid-State Circuits Conference 2002, ISSCC 2002. Digest of Technical Papers,* 2002.

[42] I. Coman, "Christian Andreas Doppler - the man and his legacy," *Eur J Echocardiogr,* 2005.

[43] M. Skolnik, "Improvements for air-surveillance radar," *IEEE Radar Conference,* 1999.

[44] K. Saunders, "CW and FM radar," *Radar Handbook 2nd ed.,* 1990.

[45] D. Banks, "Continuous wave (CW) radar," *Electron Prog,* 1975.

[46] D. Daniels, "EM Detection of Concealed Target," *Hoboken,* 2010.

[47] B. Mahafza, "Radar Systems Analysis And Design Using Matlab 3rd ed," *CRC Press,* 2013.

[48] M. I. Skolnik, "Introduction to Radar System 3rd ed," *McGraw-Hill,* 2000.

[49] E. Grayver, "Implementing Software Defined Radio," *Springer,* 2013.

[50] H. Firooz, "Implementation of full-bandwidth 802.11b receiver. http://span.ece.," 2011.

[51] A. Droitcour, O. Boric-Lubecke, V. Lubecke, J. Lin and G. Kovacs, "Range Correlation and I/Q Performance Benefits in Single-Chip Silicon Doppler Radars for Noncontact Cardiopulmonary Monitoring," *IEEE Trans. Microw. Theory Tech.,* no. 52, pp. 838-848, 2004.

[52] Y. Xiao, J. Lin, O. Boric-Lubecke and V. Lubecke, "Frequency-Tuning Technique for Remote Detection of Heartbeat and Respiration Using Low-Power Double-Sideband Transmission in the Ka-Band," *IEEE Trans. Microw. Theory Tech.,* no. 54, pp. 2023-2032, 2006.

[53] "USRP-2920 Block Diagram," National Instruments, [Online]. Available: http://www.ni.com/documentation/en/software-defined-radio-device/latest/usrp-2920/block-diagram/.

[54] Impinj, "Mini-Guardrail Antenna Datasheet," [Online]. Available: https://support.impinj.com/hc/article_attachments/115002209764/Impinj%20Miniguardrail%20Antenna%20Datasheet%20R5%2020171115.pdf.

[55] J. Sachs, "Handbook of Ultra-Wideband Short-Range Sensing," *Wiley,* 2012.

[56] A. Raffo, S. Costanzo and G. Di Massa, "Software Defined Doppler Radar as a Contactless Multipurpose Microwave Sensor for Vibrations Monitoring," *Sensors,* 2017.

[57] A. Raffo and S. Costanzo, "Doppler Elaboration for Vibrations Detection using Software Defined Radar," *Adv. Intell. Syst. Comput.,* 2017.